Mineralium Deposita
https://doi.org/10.1007/s00126-020-00994-6

ARTICLE

The formation of magnetite ores of the Glubochenskoe deposit, Turgai iron belt, Russia: new structural, mineralogical, geochemical, and isotopic constraints

Nuriya R. Ayupova[1] · Konstantin A. Novoselov[1] · Valery V. Maslennikov[1] · Irina Yu. Melekestseva[1] · Steven P. Hollis[2,3] · Dmitry A. Artemyev[1] · Svetlana G. Tessalina[4]

Received: 21 December 2018 / Accepted: 20 May 2020

Abstract

The magnetite ore bodies of the Paleozoic Glubochenskoe iron deposit (315.7 Mt at ~ 30.15% Fe) are located in the northern part of the Valerianovka arc zone ("Turgai belt") within the Transuralian Megazone, Russia. They occur in calcareous-volcaniclastic rocks, exhibit layered textures, and contain primary seafloor hematite ores. The sequence of mineral formation reflects the diagenetic to metamorphic evolution of the iron ores: (i) finely dispersed hematite-1; (ii) tabular hematite-2 crystals; (iii) pseudomorphic magnetite-1 after hematite-2; (iv) zoned magnetite-2 crystals with relict hematite-2 (or magnetite-1); (v) thin oscillatory zoned magnetite-3 crystals; and (vi) magnetite-4 porphyroblasts. A gangue assemblage of Fe-rich and Fe–Mg chlorite, illite, quartz, albite, carbonates, rutile, and apatite with rare monazite, xenotime, and zircon occurs in ore and calcareous-volcaniclastic layers. The gangue clasts (volcanic glass, Ca–Mg and Ti minerals, and altered volcanic rocks) are replaced by hematite and further by magnetite. Low siderite $\delta^{13}C$ values from layered magnetite ores (− 8.0 to − 19.5‰ PDB) indicate the presence of primary organic matter in calcareous-volcaniclastic rocks. Siderite $\delta^{18}O$ values (6.5 to 17.4‰ SMOW) are evidence of isotopic exchange between minerals and fluids during metamorphism. Negative $\delta^{34}S$ values for pyrite (down to − 4.5‰) likely indicate derivation of sulfur from organic matter in clastic sedimentary rocks. LA-ICP-MS analysis of zoned magnetite demonstrates highly variable Si, Al, Mg, Na, K, Ca, Ti, Mn, Rb, Y, Zr, Sr, U, and P contents, related to inclusions of gangue minerals. Elevated homogenous V and Ga contents and low contents of Sc, Co, Ni, Ge, As, Mo, Sn, and W (average < 5 ppm) indicate their incorporation into the structure of magnetite. All element contents (except V and Ga) are significantly higher in the inner zone of magnetite (magnetite-1) compared to the outer zone of magnetite (magnetite-2). The calcareous-volcaniclastic material, which was altered during submarine weathering and leaching, is proposed to be a major source of iron to form oxides. Altogether, the paragenetic sequence, and the mineralogical and geochemical data suggest the Glubochenskoe deposit can be characterized as a volcanic-sedimentary type of banded iron formation.

Keywords Iron ores · Hematite · Magnetite · Gangue minerals · LA-ICP-MS · Carbon and oxygen isotopes · Transuralian Megazone

Editorial handling: K. Kelley

Electronic supplementary material The online version of this article (https://doi.org/10.1007/s00126-020-00994-6) contains supplementary material, which is available to authorized users.

✉ Nuriya R. Ayupova
aupova@mineralogy.ru

[1] South Urals Federal Research Center of Mineralogy and Geoecology, Urals Branch, Russian Academy of Sciences, Institute of Mineralogy, Miass, Chelyabinsk District, Russia 456317

[2] Geological Survey Ireland, Haddington Road, Beggars Bush, Dublin 4, Ireland

[3] Irish Centre for Research in Applied Geosciences (iCRAG) & School of Earth Sciences, University College Dublin, Belfield, Dublin 4, Ireland

[4] John de Laeter Centre for Isotope Research, Curtin University, Kent St, Bentley, WA 6102, Australia

Published online: 11 June 2020

Introduction

The Turgai belt in the Transuralian Megazone of the South Urals (Fig. 1) is an exceptional iron province that hosts numerous economic deposits in volcaniclastic-sedimentary rocks of the Carboniferous Valerianovka Supergroup. The total combined resource of the deposits is estimated at > 6 Gt of iron oxide ore (Geological Survey of Russia, unpublished data). This metallogenic province is the most important iron source in Russia, although the conditions of its formation remain poorly understood. The spatial relation of magnetite deposits and intrusive rocks, the wide alteration halos of the deposits, metasomatic zonation patterns, high formation temperatures (e.g., Sarbai and Sokolovskoe deposits), and the close assemblage of magnetite with metasomatic minerals have been interpreted to indicate a metasomatic (skarn) origin for the Turgai magnetite ore (Dymkin and Prugov 1980; Bekmukhametov 1987; Herrington et al. 2002; Poltavets 2009). Recently, the ores were ascribed to the Fe skarn type, whereas late sulfides and widespread Na alteration halos of albite and scapolite suggest genetic links to the iron oxide-copper gold (IOCG) deposit class (Hawkins et al. 2017).

However, despite the extensive research of these deposits, a number of aspects of the Turgai iron deposits do not fit the "skarn" paradigm. For example, the iron ores of the Kachar deposit or the Eltai group of deposits, which occur at the same stratigraphic levels within the Late Paleozoic section, are confined to layered volcaniclastic members (Dymkin and Prugov 1980; Ivlev 2004). The layered stratabound nature of the ore bodies and their mineralogical–geochemical features indicate that iron accumulated synchronously with volcaniclastic sediments that have been subsequently metamorphosed (Dymkin and Prugov 1980; Porotov 1981). The stratabound nature and mineralogical and geochemical features are typical of most iron deposits of Silurian Tagil island arc in the Central Urals (Goroblagodatskoe, Vysokogorskoe, Evstyuninskoe) and Devonian Magnitogorsk island arc in the South Urals (Magnitogorsk ore district) (Belevtsev et al. 1982; Rudnitsky et al. 2013).

The characteristics of the hematite-bearing layers within the Glubochenskoe deposit were briefly described by Ovchinnikov and Dymkin (1987). This paper presents detailed geological, mineralogical, geochemical (including LA-ICP-MS), and isotopic ($\delta^{13}C$, $\delta^{18}O$, $\delta^{34}S$) study of magnetite

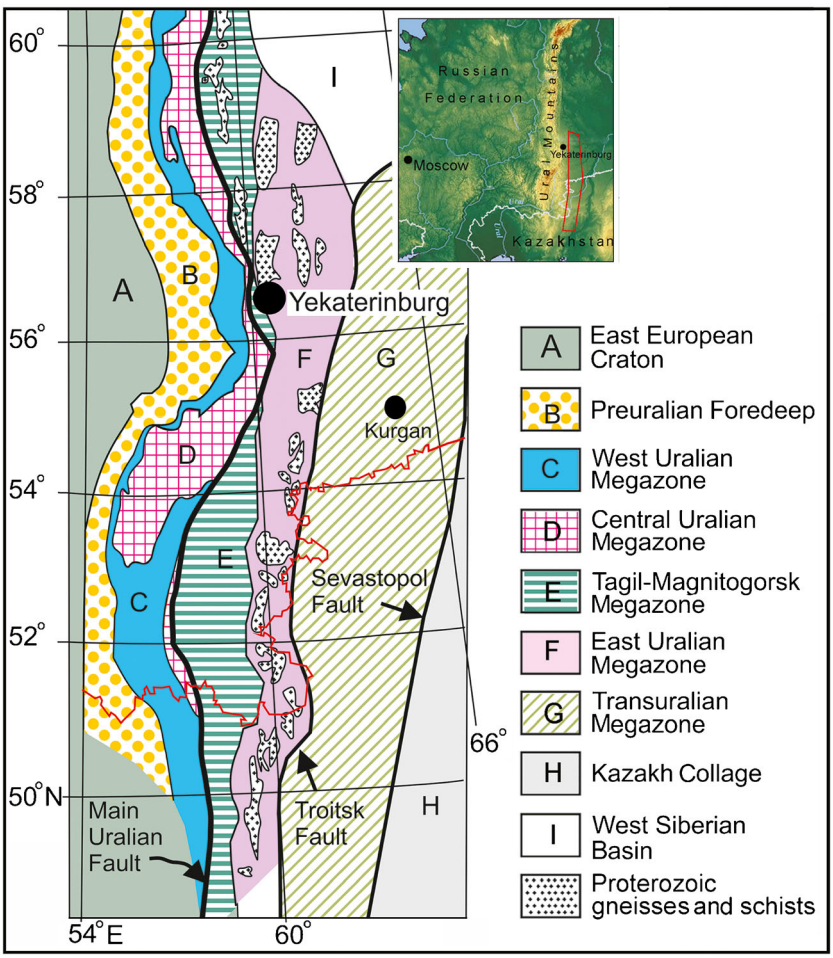

Fig. 1 Tectonic–structural map of the Southern Urals (after Puchkov 2013). The Transuralian Megazone is shown as red box in inset map. Red line is a border of Russian Federation with Kazakhstan

ore from the Glubochenskoe deposit, hosted by calcareous-volcaniclastic rocks of the Valerianovka arc zone. We have identified a primary seafloor origin for the magnetite ore, which is indicated by layered textures, the rhythmic intercalation of magnetite and calcareous-volcaniclastic layers, well-preserved relict hematite ore, and a lack of minerals typical of skarn such as pyroxene, scapolite, garnet, epidote, and actinolite. Our results contribute to a reinterpretation of other iron oxide deposits associated with volcaniclastic-sedimentary rocks worldwide.

Geological background

Regional geology

The Turgai deposits are hosted within volcanic and sedimentary rocks of the Transuralian Megazone, which is located at the junction between the Urals and Kazakhstan fold systems (Fig. 1). This megazone is separated from the East Uralian Megazone by the Troitsk Fault and the Kartaly seismic reflection zone identified in the Urals Seismic Experiment and Integrated Studies (URSEIS) and Europrobe's Seismic Reflection Profiling (ESRU) data in the west (Brown et al. 2006), and by the Sevastopol Fault of the Kazakhstan collage in the east (Puchkov 2013) (Fig. 1). The Transuralian Megazone contains pre-Carboniferous complexes, which preserve a variety of tectonic settings. These include Proterozoic (?) blocks of gneisses, crystalline schists and weakly metamorphosed sedimentary rocks, Ordovician rift (coarse terrigenous and volcanic) and oceanic (ophiolite) rocks, Silurian island-arc complexes, and Devonian deep-water rocks (Puchkov 2013). The Proterozoic to Devonian sequence of rocks is unconformably overlain by Lower Carboniferous subduction-affinity volcanogenic strata (Puchkov 2013).

The Transuralian Megazone includes from west to east: (1) the Buryktal–Dzhetygara Syncline, (2) Troitsk Anticline, (3) Aleksandrovsko–Denisovskaya Syncline–Anticline Zone, (4) Valerianovka arc zone, (5) Borovskaya Anticline, and (6) Tobol–Ubagan Uplift faulted by NNE–SSW trending faults (Ovchinnikov and Dymkin 1987; Hawkins et al. 2017) (Fig. 2). The Valerianovka arc zone hosts the iron deposits of the "Turgai belt," including the Sokolovsko–Sarbai and Kachar deposits that occur in a NNE-trending area over 800 km long and 60 km wide (Ovchinnikov and Dymkin 1987). It is separated from the Aleksandrovsko–Denisovskaya Zone in the west by the Livanovsky Fault and from the Borovskaya Anticline in the east by the Apanovsky Fault.

In the Valerianovka arc zone, early, rift-related sedimentary rock sequences are overlain by two volcano-sedimentary successions: the Valerianovka and Kachar supergroups, which indicate the transition from marine to subaerial regimes (Ovchinnikov and Dymkin 1987) (Fig. 3). The Valerianovka Supergroup (> 1000 m thick) consists of shallow marine iron-bearing calcareous-volcaniclastic-sedimentary rocks and limestones of the Sarbai and Sokolovskaya groups. The Kachar Supergroup (~ 800 m thick) locally overlies the Valerianovka Supergroup and consists of conglomerates, tuffs, and sedimentary rocks interbedded with mafic to intermediate flows of the Kurzhunkul, Andreevka, and Koshkul groups. The pyroclastic equivalents of these groups are interpreted to be largely subaerial in origin. These are in turn overlain by Mesozoic terrigenous red beds and evaporites. The rocks of Valerianovka and Kachar Supergroups are intruded by the Sokolovsko–Sarbai intrusive series (Figs. 2 and 3).

Geology of the Glubochenskoe deposit

The Glubochenskoe deposit is within the Glubochenskoe ore field in the northern part of the Valerianovka arc zone (Fig. 2), which includes three deposits (Glubochenskoe, Berezovskoe, and Petrovskoe) and a series of small occurrences. The total iron ore reserves of the ore field are estimated at 1 Gt grading 35% Fe. The deposit is not currently under exploitation.

Mineralization associated with the Glubochenskoe deposit extends 4 km and includes Southern and Northern areas (Fig. 4a). The inferred resources of the Glubochenskoe deposit are 315.7 Mt at an average Fe content of 32.20%, to a depth of 1700 m with 109.2 Mt and 206.5 Mt in the Southern and Northern areas, respectively (Orlov 2007).

The ore bodies of the Glubochenskoe deposit are hosted in the Early Carboniferous volcaniclastic-sedimentary rocks of the Middle to Upper Visean Valerianovka Supergroup, overlain by Meso-Cenozoic rocks ~ 322–345 m thick (Orlov 2007) (Fig. 4b, c). The footwall of the deposit (> 500 m thick) includes porphyritic basaltic andesite, which is intercalated with thin interlayers of fine-grained vitro- and lithic-crystal volcaniclastic rocks of the Middle Visean Sarbai Group (Orlov 2007). The basaltic andesite is greenish gray with phenocrysts (4–7%) of albitized plagioclase and pyroxene. Thin interlayers of volcaniclastic rocks are composed of clasts of basaltic andesite and plagioclase grains in a matrix dominated by devitrified volcanic glass composed of chlorite, calcite, and muscovite.

The rock sequence (up to 1500 m thick) that hosts ore is composed of fine-grained clastic calcareous-volcaniclastic sandstones, siltstones, and claystones of the lower part of the Upper Visean Sokolovskaya Group (Orlov 2007). The light gray and gray greenish, locally rhythmically banded, calcareous-volcaniclastic rocks are made up of angular clasts of plagioclase, chloritized volcanic glasses, and rare volcanic rocks and limestones, which are embedded in a siliceous–clay–carbonate matrix. The rocks contain pelitic carbonate material, locally, with foraminifera and coral relics (Ovchinnikov and Dymkin 1987).

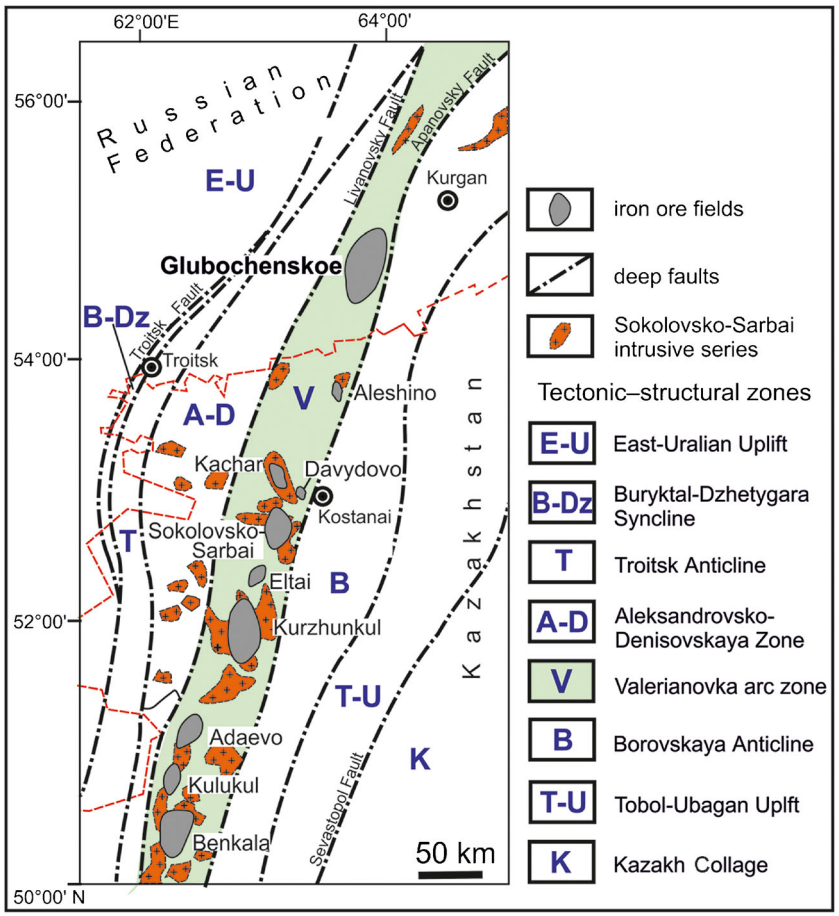

Fig. 2 Major structures of the Transuralian Megazone (after Dymkin and Prugov 1980; Herrington et al. 2002). Red line is a border of Russian Federation with Kazakhstan

The hanging-wall sequence of the deposit (up to 600 m thick) comprises limestones, polymictic breccias, and sandstones of the upper portion of the Upper Visean Sokolovskaya Group (Orlov 2007). The limestone contains abundant marine fauna including foraminifera, bryozoa, corals, ostracods, and crinoids (Ovchinnikov and Dymkin 1987).

Porphyritic diorite and gabbro form interstratal bodies, as well as necks and stocks within the host rocks, and thicker intrusions (up to 50 m) are confined to the central part of the deposit. All sedimentary and porphyric bodies are intruded by variously oriented fine-grained gabbro dikes (Fig. 4), which are equivalents to platform basalts of the Triassic Turin Group (Orlov 2007).

Magnetite ore bodies

In the Northern area of the Glubochenskoe deposit, there are a series of ore zones (> 10) at depths of 480 to 1770 m (Fig. 4a). Individual orebody thickness varies from 5 to 100 m. The Southern area contains three ore bodies at depths of 325 to 750 m, the thickness of which varies from 20 to 120 m (Fig. 4a–c). Rare magnetite-bearing rocks are exposed on the Paleozoic surface and weather to martite.

The magnetite ores are composed of rhythmically intercalated, fine-grained clastic calcareous-volcaniclastic and magnetite (rare hematite–magnetite) layers. Individual thickness of magnetite layers varies from a few millimeters up to 10 cm. Rare layers of magnetite up to 3 m thick are hosted by thicker volcaniclastic layers. Small blocks of massive ore are closely associated with epidote–chlorite–albite and albite–quartz–chlorite rocks. These rocks occur in the upper levels of the mineralized zone at the contact of subvolcanic rocks and limestones.

Analytical methods

One hundred and twenty three samples from mineralized zones and 26 samples of calcareous-volcaniclastic host rocks were collected from drill core at the Southern area of the Glubochenskoe deposit. Thirty-seven polished sections were studied by reflected and transmitted light microscopy at the Institute of Mineralogy of the South Urals Federal Research Center of Mineralogy and Geoecology, Urals Branch, Russian Academy of Sciences (IMin). The use of dark-field optical microscopic techniques allows for the identification of delicate replacement textures, which are commonly disguised in

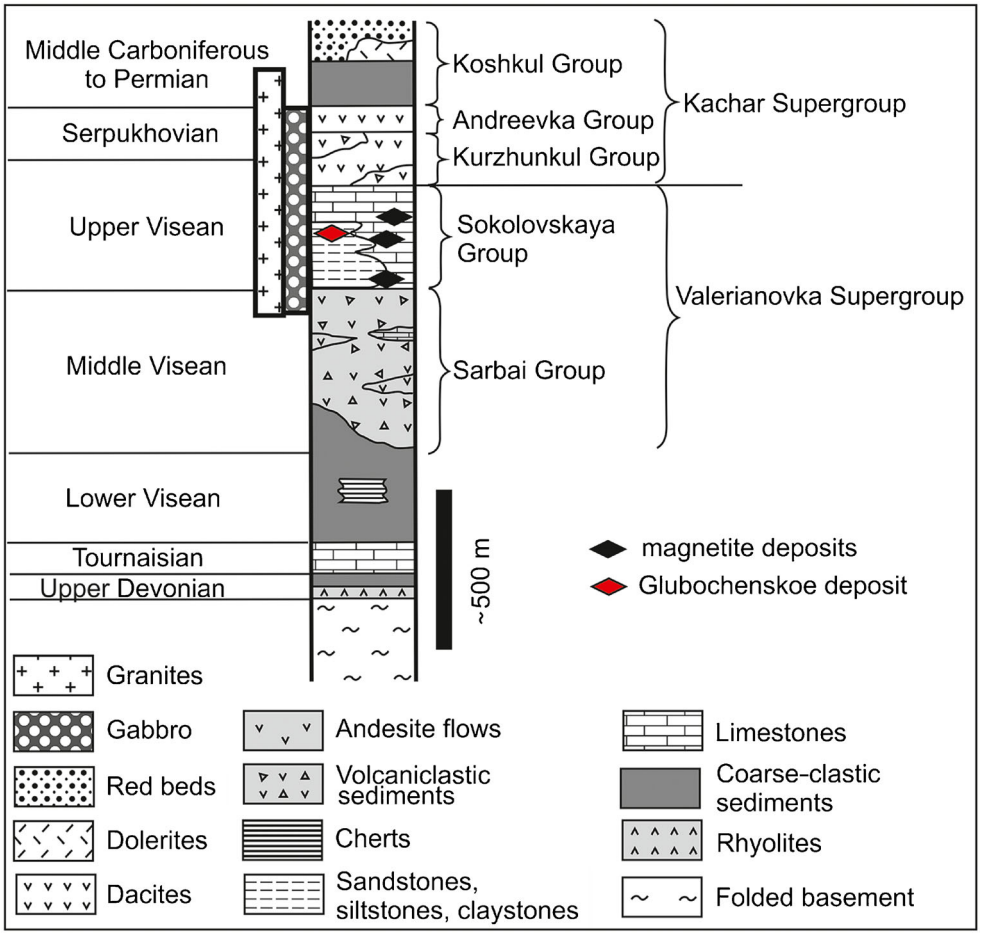

Fig. 3 Schematic stratigraphic column of the Valerianovka arc zone (after Ovchinnikov and Dymkin 1987; Hawkins et al. 2017)

fine hematite–quartz aggregates. Such textures are invisible in reflected light or transmitted light. The internal structures of magnetite and pyrite were revealed using a 2–5-s etching by concentrated HNO_3 (pyrite) and HCl (magnetite).

The bulk chemical composition of 12 host rock samples was determined by titration (Al_2O_3, FeO_{total}) with ethylenediaminetetraacetic (EDTA) acid and sulfosalicylic acid, gravimetric analysis (SiO_2) (melting of samples with $NaCO_3$ and further leaching by HCl), colorometric analysis (P_2O_5), and atomic absorption (MgO, CaO, MnO, Na_2O, K_2O) in air-acetylene flame on a PerkinElmer 3110 atomic absorption spectrometer at the IMin.

The bulk chemical compositions of magnetite ore samples were determined by X-ray fluorescence (XRF) analysis at the Russian Geological Research Institute (VSEGEI, St-Petersburg). The samples were mixed with fluxes (50% of Li metaborate and 50% of Li tetraborate) in proportion of 1:9 with the mixture melted in gold–platinum crucibles on a Classe Fluxer-Bis device (Canada). The detection limits are 0.02 wt% for SiO_2, Al_2O_3, and TiO_2; 0.01 for MnO, MgO, Fe_2O_3, Na_2O, and P_2O_5; and 0.05 for CaO and K_2O.

The trace element compositions of magnetite ore samples (Co, Cu, Ni, Zn, V, Pb, Cr, Ba, As) were determined using an OPTIMA-4300 ICP–AES (PerkinElmer) at the Russian Geological Research Institute (VSEGEI, St. Petersburg). The aqueous solutions were prepared by acid decomposition of a mixture of a sample powder (0.1 to 10 g) and flux (50% of Li metaborate and 50% of Li tetraborate) in a polytetrafluorethylene dish on electric ovens with automatic temperature regulation.

The chemical composition of minerals was analyzed on a Vega 3sbu Tescan scanning electron microscope at the IMin and a CAMECA SX 100 electron probe microanalyzer (EPMA) at the Institute of Geology and Geochemistry, Urals Branch, Russian Academy of Sciences (IGG UB RAS, Yekaterinburg). The Vega 3sbu Tescan SEM equipped with a Link ED system was operated with a 1-μm electron beam, a 15-nA beam current, a 20-kV accelerating voltage, and a counting time of 120 s. The standards used for this study are the MINM-25-53 from ASTIMEX Scientific Limited (mineral mount no. 01-044) and a registered standard no. 1362 (Microanalysis Consultants Ltd.). The EPMA used a 20-kV

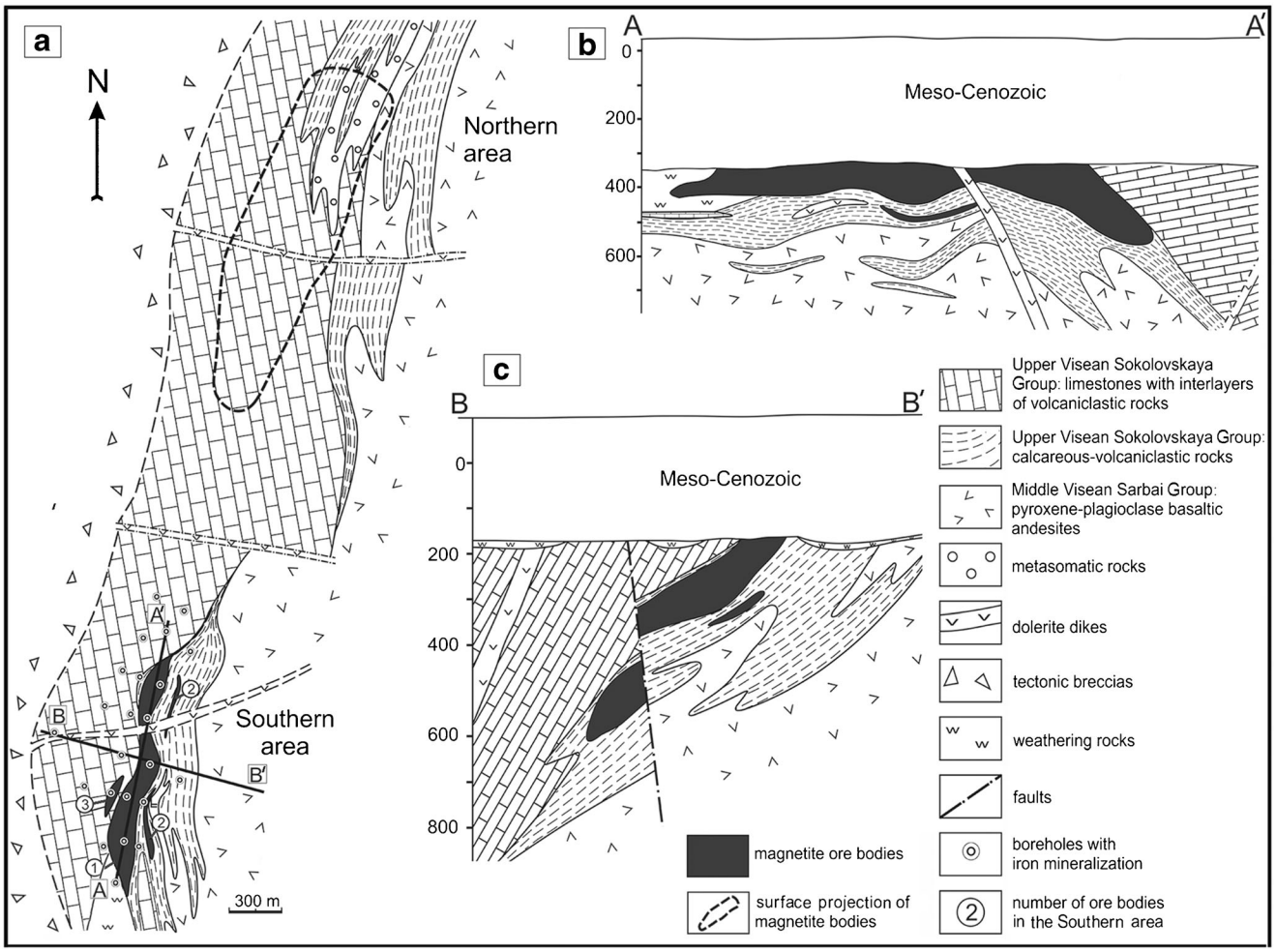

Fig. 4 Geological map (**a**) and longitudinal (**b**) and transverse (**c**) cross-sections of the Glubochenskoe iron deposit (modified after Ovchinnikov and Dymkin 1987)

accelerating voltage for Fe, Mg, Al, Ti, Cr, Mn, Zn, Co, Ca, and K and 150 kV for Si, V, and Ga, a 15-nA beam current, and a 1–3-μm beam size. The standards used are Fe_2O_3, Al_2O_3, MgO, V_2O_5, Cr_2O_3, ZnS, GaP, Ni, Co, diopside, orthoclase, rutile, and rhodonite. The analytical errors are less than (wt%) 0.15 for Fe, 0.06 for Mn, 0.04 for Al, 0.03 for Mg, Ca, and K, 0.2 for Zn, 0.1 for Ti and (ppm) 340 for Ga, 80 for V, and 40–60 for Si.

Quantitative LA-ICP-MS analysis of magnetite, pyrite, and chalcopyrite for trace elements (^{23}Na, ^{25}Mg, ^{27}Al, ^{29}Si, ^{31}P, ^{39}K, ^{42}Ca, ^{49}Ti, ^{51}V, ^{52}Cr, ^{55}Mn, ^{59}Co, ^{60}Ni, ^{65}Cu, ^{66}Zn, ^{71}Ga, ^{74}Ge, ^{75}As, ^{77}Se, ^{85}Rb, ^{88}Sr, ^{89}Y, ^{90}Zr, ^{93}Nb, ^{95}Mo, ^{107}Ag, ^{111}Cd, ^{115}In, ^{118}Sn, ^{121}Sb, ^{125}Te, ^{137}Ba, ^{179}Hf, ^{182}W, ^{197}Au, ^{205}Tl, ^{208}Pb, ^{209}Bi, ^{232}Th, ^{238}U) was carried out with a New Wave Research UP 213-nm solid-state laser microprobe coupled to an Agilent 7700X ICP-MS housed at the IMin. The analyses were performed by ablating spots ranging in size from 55 to 60 μm. Laser repetition rate was 10 Hz and laser beam energy at the sample was maintained between 3 and 4 J/cm^2. The analysis time for each spot was 75–80 s, comprising a 20–30-s measurement of background (laser off) and a 45–60-s measurement with laser on. The mass spectrometer was calibrated using multi-elemental solutions. The trace element contents were calculated in an Iolite program using international glass (BCR-2G, GSD-1G) and sulfide (MASS-1) standards and ^{57}Fe as the internal standard for quantification of magnetite (72.2%), pyrite (46.5%), and chalcopyrite (31.3%).

For isotopic studies, magnetite ores were subsampled with a diamond microdrill. The isotopic composition of S (δ^{34}S ‰ CDT) for pyrite and C (δ^{13}C ‰ PDB) and O (δ^{18}O ‰ V-SMOW) for carbonates was analyzed on a Delta+ Advantage, Thermo Finningan mass-spectrometer equipped with an EAFlash 1112 elemental analyzer and ConFloIII interface housed at the IMin using NBS-123 standard for S (sphalerite, US National Bureau of Standards) and NBS-18, NBS-19, and IAEA-C-3 standards for C and O. The analytical error is ± 0.1‰ for S, 0.06 for C, and ± 0.2‰ for O. The results were processed in the ISODAT-2.0 program.

Results

Textures of magnetite ores

Magnetite ore from the Southern area of the Glubochenskoe deposit is characterized by variable proportions of massive, brecciated, and layered textures. Massive ore is composed of granular aggregates of magnetite with stringer-disseminated sulfides, and a quartz, calcite, and chlorite matrix (Fig. 5a). Brecciated sulfide-magnetite zones with similar mineralogy to massive ore host angular quartz–calcite clasts (Fig. 5b) and locally exhibit vague layered textures. In cross-section, the brecciated zones gradually transit laterally to layered ore with an intercalation of magnetite and host rock layers. The contrast between the layers is emphasized by the intense alteration of locally faulted volcaniclastic quartz–chlorite–albite layers (Fig. 5c).

Layered textures are the most abundant (> 70%) and are found throughout the orebody and consist of intercalation of magnetite and fine-grained chlorite–calcite–quartz calcareous-volcaniclastic layers (Fig. 5d). In many places, fine-grained magnetite-bearing layers grade to massive magnetite–quartz–chlorite layers. Locally, these massive layers mimic host rock textures. The contacts between magnetite and calcareous-volcaniclastic layers are sharp on bottom and gradational in the upper parts of the calcareous-volcaniclastic layers (Fig. 5e, f). The host rock layers contain finely disseminated magnetite. In some layered ores, the magnetite layers are characterized by various thickness, grain size, and proportion of magnetite and host rock components. The calcareous-volcaniclastic layers contain fragments of plagioclase, quartz grains, and chloritized volcanic glasses, which are cemented by a chlorite–carbonate–quartz assemblage.

The layered magnetite-bearing siltstones and claystones (Fig. 5g) at the top of the ore bodies are characterized by variable amounts of magnetite, a rhythmic alternance of fine-grained magnetite (±hematite), calcareous-volcaniclastic layers, and large semi-rounded clasts of magnetite ore and limestones. The latter deform the underlying layers.

Some ore intervals are characterized by the intercalation of fine-grained hematite and calcareous-volcaniclastic layers or by the intercalation of calcareous-volcaniclastic layers variously enriched in hematite (Fig. 5h). The hematite layers contain numerous angular silicified and chloritized clasts of volcanic glass. The layers exhibit wavy surfaces and variable thickness with local swells, as well as load casts on hematite layers.

Chemical composition of host rocks and magnetite ores

The calcareous-volcaniclastic layers are characterized by up to relatively high Al_2O_3 (17.78 wt%), TiO_2 (1.41 wt%), CaO (7.11 wt%), Na_2O (7.17 wt%), and P_2O_5 (0.58 wt%) and low MgO (5.78 wt%) and MnO (0.13 wt%) contents (ESM 1). The K_2O content is generally low, although it is as high as 4.09 wt% in some layers. The total iron content (Fe_2O_3+FeO) varies from 2.12 to 13.68 wt%, and the C_{org} content of siltstones ranges from 0.11 to 6.98 wt%.

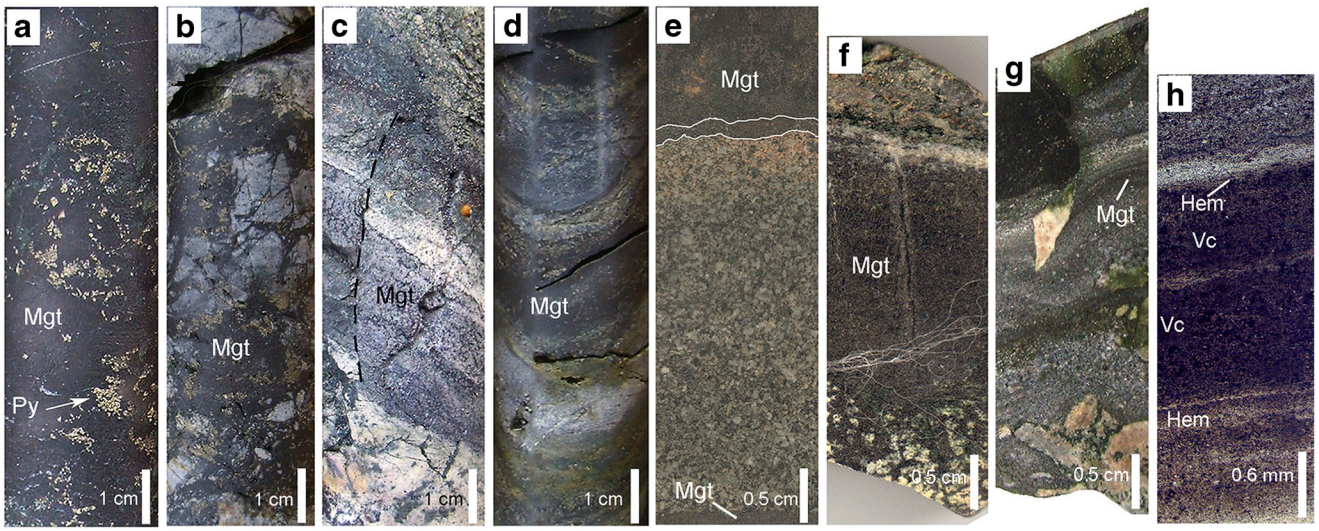

Fig. 5 Textures of magnetite ore in drill core from the Glubochenskoe deposit. **a** Massive fine-grained magnetite (Mag) ore with disseminated pyrite (Py). **b** Brecciated ore with abundant sulfides and fractured quartz–carbonate clasts (gray–white). **c** Layered ore showing intercalated magnetite and calcareous-volcaniclastic (white-green) layers with vertical displacement by fault. **d** Rhythmic intercalation of magnetite and fine-grained clastic chlorite–calcite–quartz calcareous-volcaniclastic layers. **e** Rhythmic intercalation of calcareous-volcaniclastic and magnetite layers with volcaniclastic relics (partly magnetitized layer in the top of the volcaniclastic layer is highlighted by white color). **f** Chlorite–albite–quartz–carbonate calcareous-volcaniclastic layer showing gradational contact at top and sharp contact at bottom with magnetite. **g** Silty layers with fragments of coarse magnetite and limestone clasts. **h** Intercalated fine-grained hematite (in up to 1–2-mm-thick layers) and calcareous-volcaniclastic layers that are variously enriched in hematite. Drill core sample

The Fe_2O_3+FeO content of magnetite-rich samples varies from 28.7 to 77.9 wt% (ESM 2). All massive, brecciated, and layered ores are characterized by relatively high SiO_2 contents (32.77 wt%, on average). The total Fe content is negatively correlated with major oxides with decreasing ranges as follows: 53.8 to 13.3 wt% SiO_2, 15.70 to 1.41 wt% Al_2O_3, 6.49 to 0.13 wt% MgO, and 0.84 to 0.11 wt% TiO_2 (Fig. 6a–c). The Al_2O_3 and TiO_2 contents correlate positively (r^2 = 0.90) (Fig. 6d). Magnetite ore samples contain P_2O_5 (0.05–0.42 wt%; ESM 2) and, in some samples, P_2O_5 is positively correlated with Al_2O_3 and TiO_2 contents. The Na_2O content is highly variable (from 0.05 to 3.89 wt%) but is positively correlated with Al_2O_3 (r^2 = 0.74) and TiO_2 (r^2 = 0.69) contents (Fig. 6e, f). The K_2O content of the ores is low (0.20 wt%, on average).

Mineral assemblages of ore

Magnetite and hematite

Magnetite and hematite are the major iron minerals of the Glubochenskoe deposit. Magnetite occurs in amount from 20 vol% in brecciated and layered ores to 90 vol% in massive ores. Hematite occurs in some magnetite-rich calcareous-volcaniclastic horizons, rarely forming monomineralic layers. Several generations of iron oxides have been identified. Rare, fine-grained hematite-1 associated with quartz-1 replaces the volcanic glass (Fig. 7a) and occurs in the matrix of some ore layers. In hematite-rich layers, variously oriented tabular hematite-2 crystals form massive aggregates in a quartz matrix (Fig. 7b). In some cases, tabular hematite-2 forms extremely

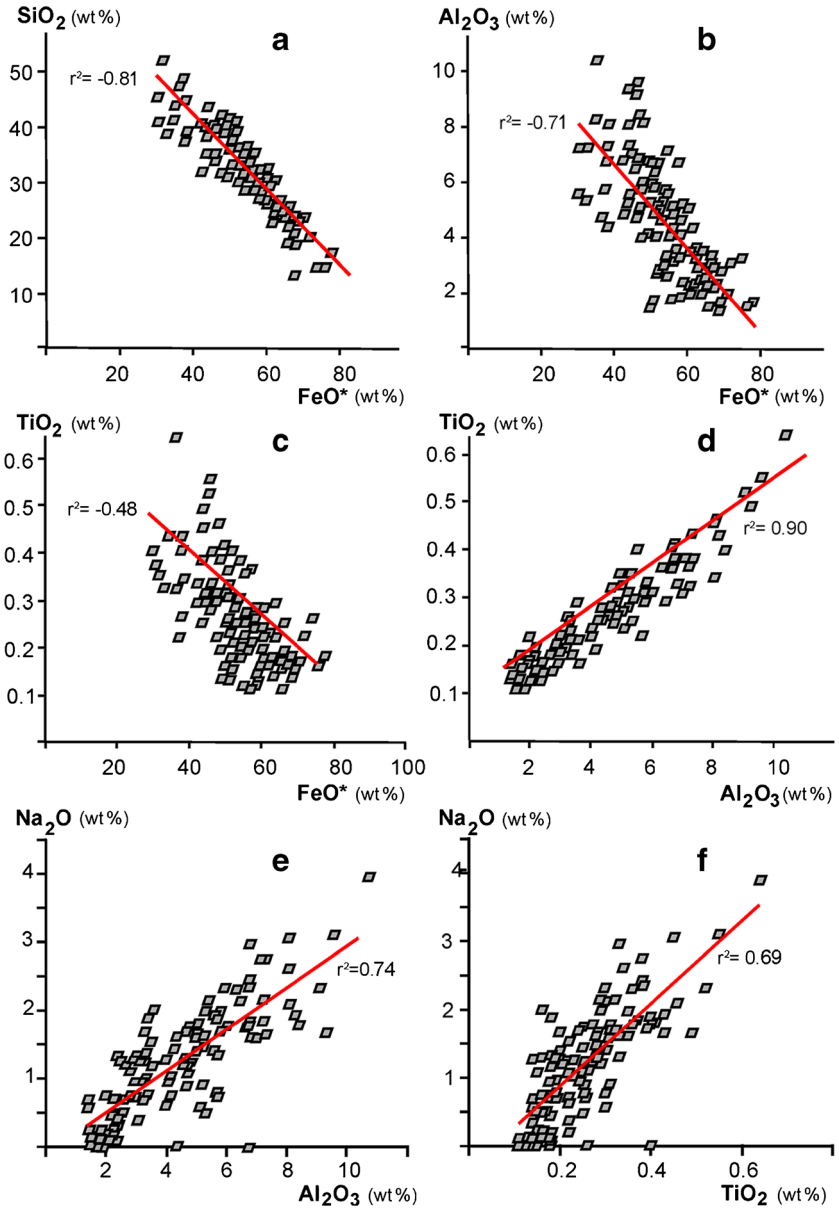

Fig. 6 Bivariate plots of major oxides of magnetite-rich samples from the Glubochenskoe deposit

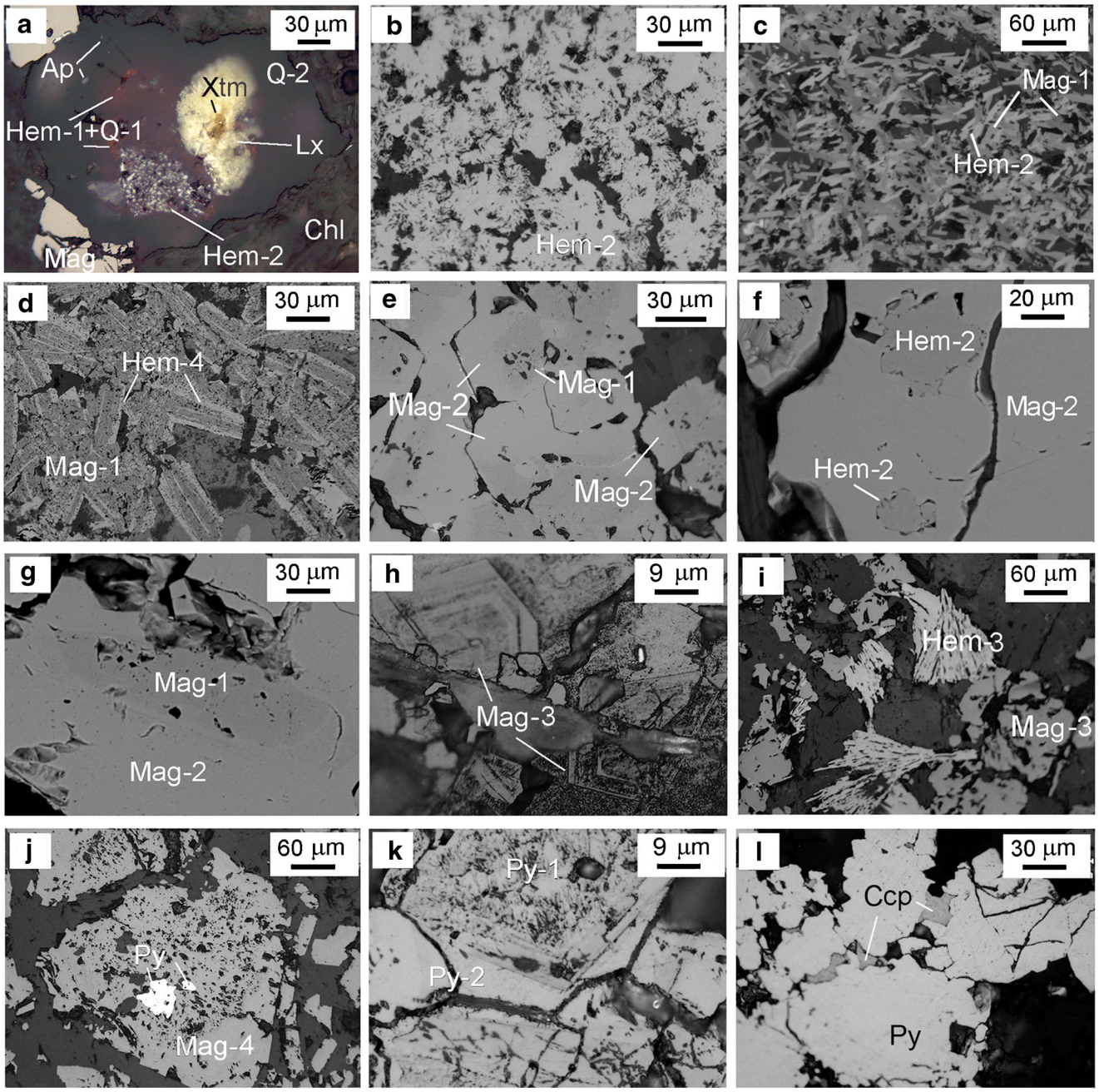

Fig. 7 Microtextures of magnetite ores from the Glubochenskoe deposit. **a** Finely dispersed hematite-1–quartz-1 intergrowth (Hem-1+Q-1), crystalline hematite-2 (Hem-2), and leucoxene (Lx) with inclusions of xenotime (Xtm) and apatite (Ap) in volcanic glass inside Fe-rich chlorite matrix. **b** Massive aggregates of tabular hematite-2 (light gray) in quartz matrix (dark gray). **c** Reduction of hematite-2 (light gray) to magnetite-1 (Mag-1) in quartz–silicate matrix. **d** Pseudomorphic magnetite-1 after hematite-2, which is replaced by hematite-4 (Hem-4). **e** Zoned magnetite with early heterogeneous magnetite (Mag-1) and late homogeneous magnetite (Mag-2). **f** Hematite-2 inclusions in central zone of magnetite-2 grains. **g** Tabular magnetite-1 in inner zone of magnetite-2. **h** Fine-zoned euhedral magnetite-3 (Mag-3) crystals in massive ores (after etching). **i** Assemblage of fibrous hematite-3 (Hem-3) and magnetite-3 (Mag-3) in quartz–carbonate–silicate matrix. **j** Inclusion of pyrite (Py) in magnetite-4 (Mag-4) porphyroblasts. **k** Porous pyrite-1 grains overgrown by subhedral pyrite-2 (after etching). **l** Anhedral chalcopyrite (Ccp) between pyrite grains. Photo **a**–**e** and **h**–**l** reflected light, **f**–**g** BSE images, and **h**, **k** etched by HCl_{conc}

fine, curved flakes and is partly or totally pseudomorphically replaced by tabular magnetite-1 crystals (Fig. 7c, d). In calcareous-volcaniclastic layers, the acicular crystals or anhedral aggregates of hematite-2 occur between volcanic clasts. Hematite-2 associated with tabular magnetite-1 crystals is also observed inside volcanic clasts.

Subhedral zoned magnetite crystals (up to 60–100 μm) form massive layers and consist of a strongly porous inner

zone (magnetite-1) domain (30–40 μm thick) with abundant inclusions of silicates, quartz, rutile, and homogeneous outer zone (magnetite-2) (20–50 μm thick) (Fig. 7e). In some magnetite layers, the inner zone of magnetite crystals is occupied by porous hematite-2 (Fig. 7f) or pseudomorphic tabular magnetite-1 crystals (Fig. 7g).

Euhedral magnetite-3 crystals from massive ore are finely zoned (Fig. 7h). Locally, magnetite-3 crystals are associated with hematite-3, which occur as sheaf and fan-like aggregates (Fig. 7i). Fractured massive magnetite-4 porphyroblasts, which host pyrite inclusions (up to 300–400 μm), are characterized by less dense and heterogeneous inner cores and more compact outer rims (Fig. 7j).

In the southern flank of the ore body, subhedral zoned magnetite crystals are pseudomorphically replaced by hematite-4 (Fig. 7d), within lenses of martite ores. Martite replaces magnetite from crystal margins and along the octahedral structural planes. This occurred after the formation of porphyroblastic magnetite-4.

Sulfide minerals

Pyrite is the most common sulfide mineral in the Glubochenskoe magnetite ore samples. It forms uneven disseminations of coalesced subhedral to euhedral crystals, and fine- to medium-grained granular aggregates. This dissemination is subparallel to layering and locally forms massive interlayers at the contact between ore and host rock. In massive ores, pyrite locally contains inclusions of magnetite and pyrite inclusions are typical of magnetite porphyroblasts (Fig. 7j). Etching shows that pyrite is zoned with a porous core (pyrite-1) and a more compact outer zone (pyrite-2) (Fig. 7k). In martite-rich samples, pyrite is replaced by goethite. Chalcopyrite occurs as interstitial aggregates in subhedral pyrite crystals (Fig. 7l). It also rims pyrite grains in assemblages with magnetite-3 and hematite-3.

Mineral assemblages and chemical composition of gangue minerals

The calcareous-volcaniclastic and (hematite)–magnetite layers are characterized by clastic structure and similar gangue mineral assemblages. Quartz is the most abundant non-opaque mineral in magnetite (hematite) ores and calcareous-volcaniclastic layers (Figs. 7a and 8a–c, f) and forms at least three generations. Microcrystalline quartz-1 is closely associated with finely dispersed hematite-1 in volcanic glasses and in the matrix of some magnetite layers (Fig. 7a). Quartz-2 occurs as angular clasts in the matrix of magnetite (hematite) and calcareous-volcaniclastic layers or forms the groundmass in assemblages with other minerals (Fig. 8a–c). Quartz-2 replaces volcanic glass, Ca–Mg minerals, Ca-plagioclase, and K-feldspar and is associated with crystalline hematite-2 (Fig. 8c). Quartz clasts exhibit heterogeneous inner structure because of inclusions of chlorite, calcite, leucoxene, rare apatite, xenotime, monazite, and zircon (Fig. 8c). Interstitial quartz-3 occurs in massive magnetite ores.

The volcaniclasts and the groundmass of the magnetite and calcareous-volcaniclastic layers show extensive alteration to chlorite. Chlorite comprises 5–10% of magnetite layers and 20–30% of calcareous-volcaniclastic layers and includes Fe-rich (FeO_{total} is > 30 wt%) and Fe–Mg types (ESM 3). Fine scaly anhedral aggregates of dark fibrous and laminar Fe-rich chlorite are closely associated with zoned magnetite-2 crystals (Fig. 8c). Chlorite also occurs with siderite and apatite between volcanic glasses and plagioclase clasts (Fig. 8d). The Fe-rich chlorite in this sample is characterized by high Fe/(Fe+Mn) values (0.68–0.77) and low MgO contents (6.22–9.68 wt%).

Fe–Mg chlorite with Fe/(Fe+Mn) values of 0.32–0.42 is associated with illite (up to 2–3 μm wide), where illite forms platy grains up to 100 μm in size (Fig. 8e, ESM 3) or replaces detrital K-feldspar and plagioclase fragments. In contrast to the Fe–Mg chlorite of magnetite ore from the Kachar, Sokolovskoe, and Sarbai deposits (Hawkins et al. 2017), that of the Glubochenskoe deposit has minor MnO (0.11–0.19 wt%) and CaO (0.01–0.24) contents (ESM 3). None of the analyzed chlorites contained detectable Na_2O, K_2O, and TiO_2 contents in contrast to metasomatic skarns, which typically contain high contents of these major oxides (Hawkins et al. 2017). On the basis of chlorite geothermometry (Kranidoitis and MacLean, 1987), the formation temperature of Fe-rich and Fe–Mg chlorite is 184–217 and 230–266 °C, respectively (Table 3).

Feldspar group minerals form angular clasts up to 0.2 mm in size with corroded boundaries. Plagioclase (3.02–7.14 wt% CaO) is characterized by polysynthetic twins, whereas K-feldspar exhibits simple twins. The fragments of K-feldspar are completely or partly replaced by the newly formed albite–illite–quartz assemblage and Ca-plagioclase replaced by albite (Fig. 8b, e).

Siderite forms microlayers or anhedral aggregates between other minerals in samples containing magnetite-2 (Fig. 8d, e). It contains minor amounts of CaO (1.86–2.03 wt%), MgO (0.00–0.47 wt%), and MnO (2.24–2.75 wt%) (ESM 4). Mg–Fe carbonate (ankerite) is associated with quartz in the matrix of magnetite ore samples (Fig. 8f) and has a negligible MnO content (0.45–0.97 wt%) (ESM 4).

Numerous large calcite clasts (up to 300–500 μm in size) are typical of calcareous-volcaniclastic layers. In the groundmass of magnetite layers, fine-grained calcite grains are typically intergrown with chlorite–quartz (±illite) aggregates. Calcite exhibits low MnO (up to 3.32 wt%) and FeO (up to 2.40 wt%) contents (ESM 4).

Rutile grains up to 25 μm in size, intergrown with Mg–Fe carbonate, are interstitial to magnetite grains. Local clusters of

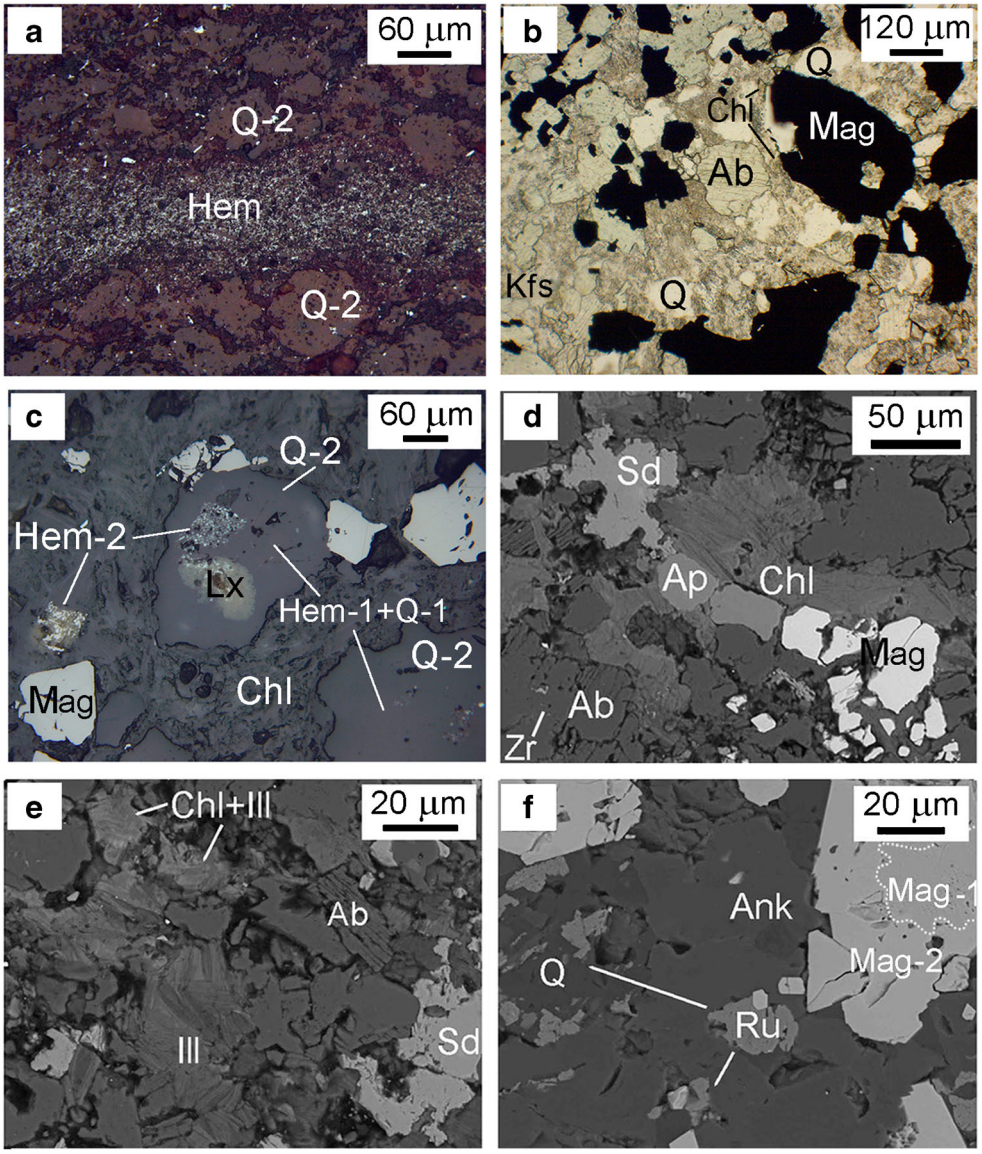

Fig. 8 Gangue mineral assemblages of magnetite ores from the Glubochenskoe deposit. **a** Detrital quartz grains (Q-2) cemented by quartz (±chlorite–carbonate) in calcareous-volcaniclastic layers with hematite (Hem) layer. **b** Clastic quartz, albite (Ab), chlorite (Chl), and feldspar (Kfs) with vague boundaries in chlorite–quartz–carbonate matrix. **c** Fibrous Fe-rich chlorite forming the matrix of volcaniclastite. **d** Fe-rich chlorite–siderite (Sd)–apatite (Ap) assemblage between albite, quartz, and carbonate clasts (Zr—inclusions of zircon in albite). **e** Alternation of Mg–Fe chlorite and illite (Ill) plates and albite fragments with anhedral siderite. **f** Anhedral aggregates of ankerite (Ank), quartz and rutile (Ru) between magnetite-2 (Mag-2). Photos **a** and **c** reflected light and dark field, **b** transmitted plane-polarized light, and **d**, **e**, **f** BSE images

leucoxene were identified in the matrix of volcaniclastic layers and occur (up to 120 μm) in partly hematitized volcanic glasses and Ca–Mg minerals (Fig. 8c).

Altered volcanic clasts contain numerous inclusions of apatite, xenotime, and zircon (Fig. 8c). Isometric grains of apatite (5–20 μm) and monazite (up to 5 μm size) (wt%: 32.80 P_2O_5, 0.27 CaO, 1.27 FeO, 26.34 Ce_2O_3, 22.48 Nd_2O_3, 8.68 La_2O_3, 3.95 Pr_2O_3, 3.55 Sm_2O_3) locally occur in the matrix of magnetite layers. Accessory zircon (1–3 μm in size) is found as inclusions within twinned plagioclase crystals (Fig. 8d).

Chemical composition of ore minerals

Magnetite

EPMA shows that the inner (magnetite-1) and outer (magnetite-2) zones of magnetite grains are characterized by variable contents of Si (0.007–0.092 wt%) and V (0.005–0.038 wt%), as well as Mg, Al, Mn, Ti, K, Zn, Ni, Ca, Cr, and Ga (ESM 5). The average Ti, Ca, and Zn contents in magnetite-1 are higher in comparison with magnetite-2 (ESM 5).

The LA–ICP–MS analyses demonstrate greater variability of trace element contents compared to EPMA due to large laser beam size: results of magnetite-1 reflect captured inclusions of quartz, chlorite, illite, albite, and rutile, which have been observed by optical microscopy. Sporadic high maximum concentrations include Sr (23.7 ppm), Sb (278 ppm), Cr (48.4 ppm), Co (14.80 ppm), Ni (6.79 ppm), Sc (10.37 ppm), and Ba (9.40 ppm). The Ga (22.2–34.9 ppm) and V (73.3–84.3 ppm) contents are less variable. Low contents (average < 2 ppm) are typical of Rb, Zr, Y, U, Ge, As, Mo, Sn, W, Pb, Bi, Th, Ag, and Au (ESM 6).

High Si, Mg, Al, K, Ti, Na, and Ca contents are also characteristic of magnetite-2; however, average abundances are 3.6–15.8 times lower than those in magnetite-1 (ESM 6). The contents of other trace elements in magnetite-2 are either similar or slightly lower compared to magnetite-1 (ESM 6). LA–ICP–MS analysis of magnetite shows positive Al–Si, Al–Mg, Al–K, Na–Ca, Ca–Sr, Sr–U, K–Rb, K–Zr, and K–Y correlations (Fig. 9).

Pyrite and chalcopyrite

Pyrite from magnetite ore samples is characterized by highly variable Co (31–2350 ppm) and Ni (24–711 ppm) contents (ESM 7). The Co contents are higher in the outer zone of pyrite grains (pyrite-2, average 999 ppm) compared with that in the core (pyrite-1, average 116 ppm). The Ni contents are widely variable in both the core (43–476 ppm) and in the outer zone (24–711 ppm), and there is little or no correlation between Co and Ni. The Co/Ni ratios of pyrite vary widely from 0.24 to 28.85 (Fig. 10a): 0.24–0.97 in the core and 1.52 up to 28.25 in the outer zone. Rare extremely high Cu contents (1220–22000 ppm) are also confined to the outer zone of pyrite grains and reflect microinclusions of chalcopyrite. In the core and the rim of pyrite, Se (13.10–43.50 ppm), As (1.40–22.80 ppm), Zn (0.70–7.20 ppm), and Mn (0.001–24.0 ppm) exhibit variable contents, whereas V, Cr, Ga, Ge, Mo, Ag, Sn, Sb, Te, Pb, and Bi contents are extremely low (average ≤ 1 ppm).

Cobalt, Ni, and As in chalcopyrite show limited ranges in concentrations (average 0.14, 0.51, and 0.69, respectively) (ESM 7). The Se contents (average of 35 ppm) are comparable

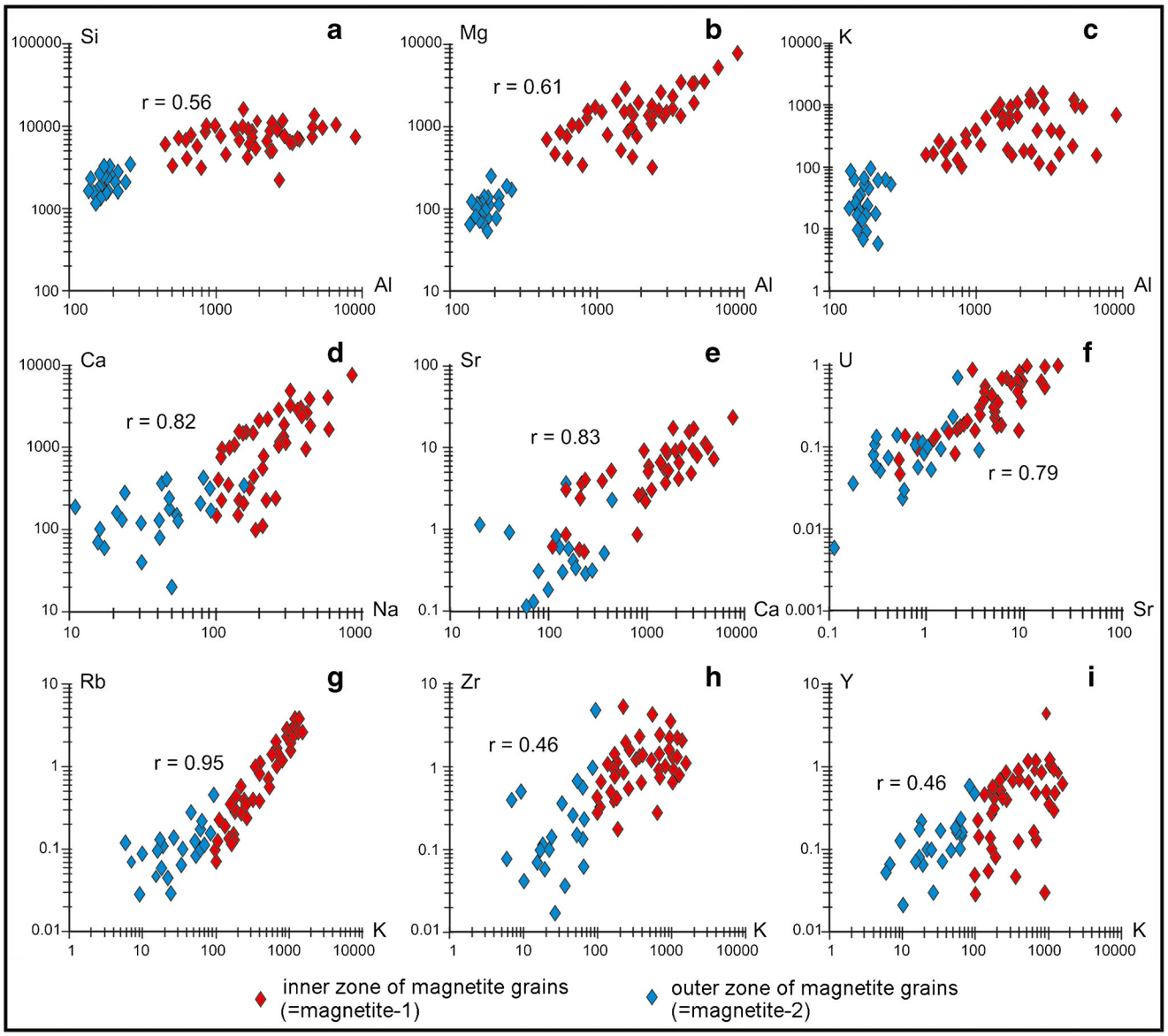

Fig. 9 Plots of trace elements in magnetite determined by LA-ICP-MS analyses. All values in parts per million

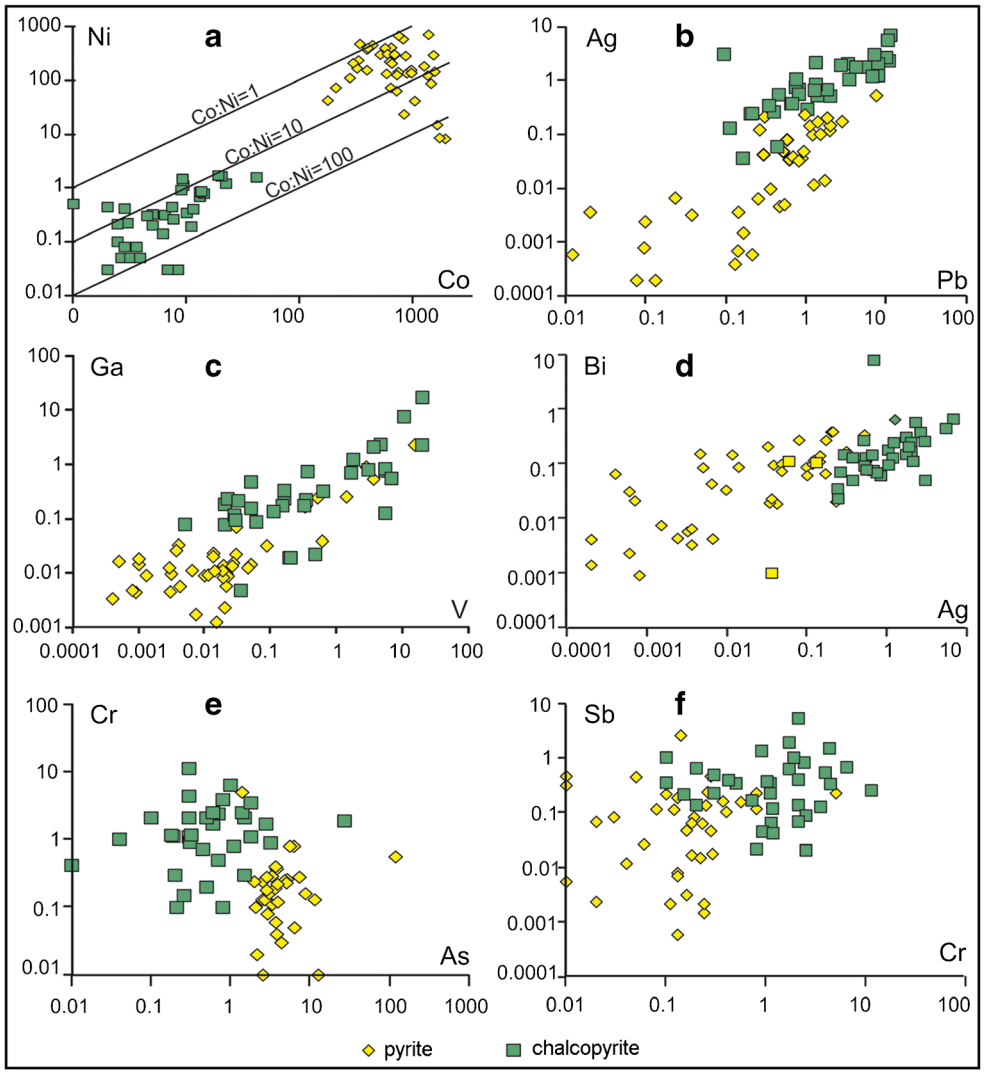

Fig. 10 Plots of trace elements in pyrite and chalcopyrite determined by LA-ICP-MS analyses. All values in parts per million

with those of pyrite, whereas the concentration ranges of some trace elements are higher than in pyrite (V, Cr, Ge, Sn, Te, Bi, and locally, Mn, Zn, Ga, Ag, Sb, and Pb) (Fig. 10).

S, C, and O isotopic composition

Pyrite from magnetite samples yields $\delta^{34}S$ values from − 4.5 to + 3.6‰ (ESM 8). The lowest values are typical of pyrite from layered samples (− 4.5‰) (Fig. 11a). Pyrite from brecciated magnetite ores is characterized by positive $\delta^{34}S$ values (up to + 3.6‰). Pyrite from massive magnetite zones exhibits intermediate $\delta^{34}S$ values (from + 0.6 to + 2.6‰).

Siderite, which is the dominant carbonate species in the layered magnetite samples, has $\delta^{13}C$ values from − 8.0 to − 19.5‰ and $\delta^{18}O$ values from 6.5 to 17.4‰ (ESM 8; Fig. 11b). The negative $\delta^{13}C$ values of calcite from massive, brecciated ores, and layered ores vary from − 6.4 to − 12.2‰ (Fig. 11b). The $\delta^{18}O$ values of carbonates from massive ores range from + 2.4 to + 7.6‰. The $\delta^{18}O$ values of carbonates from brecciated and layered samples are higher (+ 8.4 to + 14.7‰) (Fig. 11b).

Discussion

Magnetite ores from the Glubochenskoe iron deposit have a unique set of geological features atypical of most magnetite skarn deposits in the Valerianovka arc zone (Dymkin and Prugov 1980; Bekmukhametov 1987; Herrington et al. 2002; Poltavets 2009; Hawkins et al. 2017). These features include (i) the lack of intrusive igneous rocks within ~ 130 km of the deposit (Fig. 2), (ii) fine-grained calcareous-volcaniclastic rocks are the sole host rocks, (iii) the stratabound ore and abundance of layered textures, (iv) the presence of primary hematite mineralization, and (v) the absence of typical skarn minerals such as pyroxene, scapolite, garnet, epidote, and actinolite (Figs. 5, 7, and 8). The layered textures, well-preserved calcareous-volcaniclastic layers,

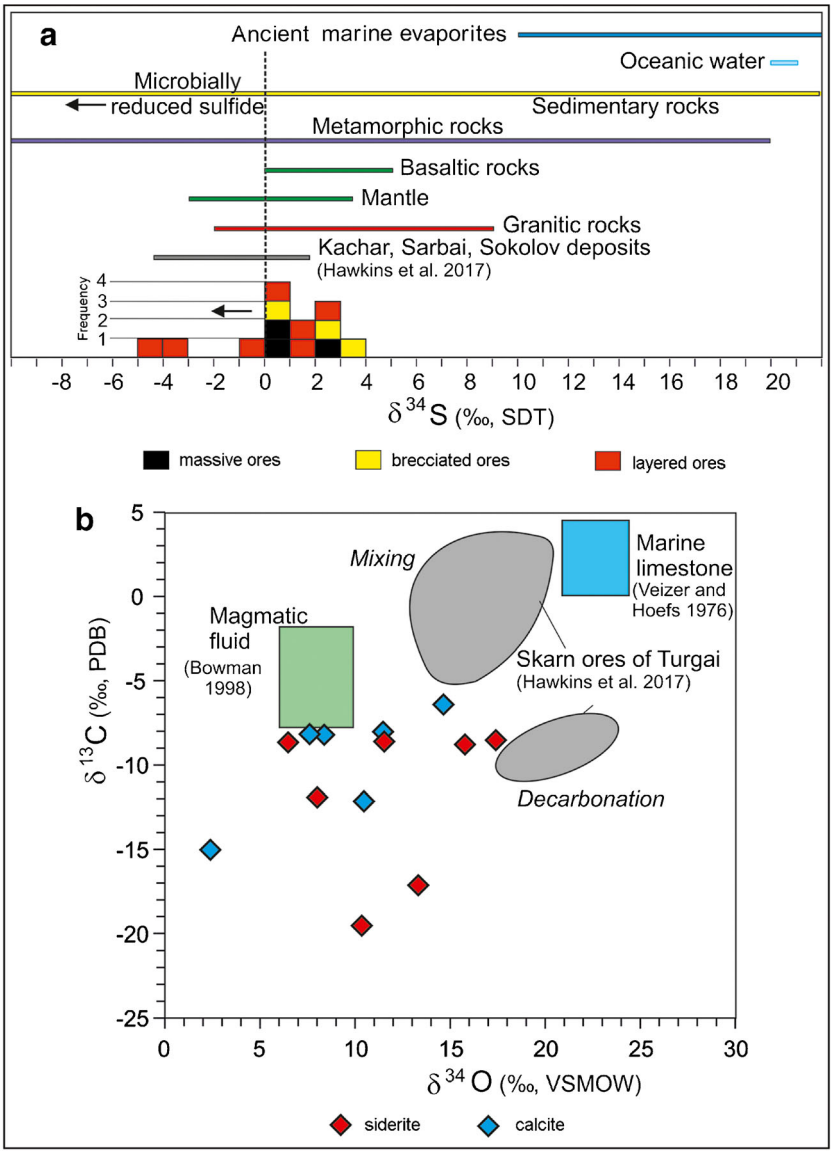

Fig. 11 **a** Sulfur isotopic composition ($\delta^{34}S_{CDT}$) of pyrite from massive, brecciated, and layered magnetite ores of the Glubochenskoe deposit in comparison with $\delta^{34}S_{CDT}$ values of major Earth reservoirs (Ohmoto and Rye 1979; Alirezaei and Cameron 2001) and pyrite of the Kachar, Sarbai, and Sokolov skarn deposits (Hawkins et al. 2017). **b** Carbon ($\delta^{13}C$, PDB) and oxygen ($\delta^{18}O$, VSMOW) isotopic composition of calcite and siderite from the Glubochenskoe deposit in comparison with $\delta^{13}C$, PDB and $\delta^{18}O$, VSMOW values of various reservoirs. Our results for Glubochenskoe carbonates differ from the results of Hawkins et al. (2017) for Turgai belt skarn deposits in that they extend to much lower 18-O and 13-C compositions

gangue clasts, and the mineral composition of gangue clasts (chlorite, illite, carbonates, and albite) indicate the host rocks experienced only greenschist facies metamorphism. The top and bottom wavy boundaries of hematite layers and load signs of clastic material in hematite layers indicate that the hematite layers formed prior to the lithification of ore sediments. All these features are consistent with primary sedimentary layering rather than high-grade metamorphic segregation or metasomatic-skarn mobilization of iron ores.

Formation of Fe oxyhydroxides and hematite

The well-preserved hematite layers, finely dispersed Fe–Si aggregates, and hematite-2 crystals in magnetite layers indicate a primary Fe oxyhydroxide origin of the Glubochenskoe deposit (ESM 9). Amorphous Fe oxyhydroxides in assemblages with silica and Fe–Mg smectites are major components of Fe oxyhydroxide sediments on the present-day seafloor. Such deposits preferentially form in proximity to low- to moderate-temperature hydrothermal fields (Taitel-Goldman and Singer 2002; Cuadros et al. 2013; Kiyokawa and Ueshiba 2015). These amorphous Fe sediments can be converted to hematite during diagenesis at temperatures of 70 to 140 °C (Fischer and Schwertmann 1975; Maynard 1983). Some authors indicate that alteration of volcaniclastic material such as lithic fragments, feldspars, volcanic glass, or ferromagnesian silicates by interaction with seawater can also produce Fe oxyhydroxides and clay mineral assemblages (e.g., Petrova et al. 1980; Kossovskaya et al. 1982). Reed (1983) has shown that, in seawater-basalt reactions, ferrous Fe can be oxidized by sulfate and stored in ferric hydroxide complexes until hematite is transformed. Some oolitic Fe ores

are also considered the products of submarine weathering of volcanic ash (Sturesson 2003). The seafloor transformation of hyaloclasts through Fe–Mg smectites to hisingerite $Fe_2Si_2O_5(OH)_4{\cdot}2H_2O$ as precursors of fine-grained hematite-quartz intergrowths has also been well documented from ferruginous sedimentary rocks in volcanogenic massive sulfide deposit districts of the Urals (Maslennikov et al. 2012). Hematite is widely regarded to be "primary" in banded iron formations (BIF), derived from hydrous ferric oxyhydroxides during dehydration, although some hematite may have formed from diagenetic silicates (Kaufman and Hayes 1990).

Transformation of hematite to magnetite

It is likely that ferric iron, and dissolved/absorbed ferrous iron, combined to form a mixed valence Fe phase that was later converted to magnetite during late diagenesis. Several magnetite layers examined in thin section appear to have been completely unaffected by metamorphism, in particular, those that contain magnetite-2 enclosing hematite-1 or magnetite-1. It is known that, under variable O contents, magnetite pseudomorphically replaces hematite at low temperatures (Ramdohr 1969). Experimental studies have also shown that the phase transformation of α-Fe_2O_3 to Fe_3O_4, the reduction of Fe^{3+} to Fe^{2+}, and the nucleation and growth of new polyhedral particles of Fe_3O_4 occurs at temperatures of 160 to 220 °C (Lu and Tsai 2015). Most models of BIF formation involve the primary precipitation of hydrated amorphous Fe-oxides that are progressively transformed, first to hematite and then eventually to magnetite (Maynard 1983; Brown et al. 1995; Bontognali et al. 2013). In models involving the oxidation of buried organic matter, the reduction of Fe(III) is interpreted to have been the source of Fe(II) for magnetite formation (Posth et al. 2013). The presence of organic carbon (up to 6.98 wt%) (ESM 1) in calcareous-volcaniclastic siltstones of the Glubochenskoe deposit may have caused the transformation of primary Fe oxyhydroxides into magnetite through oxidation of organic matter.

Hematite can also be transformed to magnetite through reaction with reduced fluids in unlithified sediments. The large volume increase accompanying this reaction can only be accommodated in unconsolidated material (Mucke and Cabral 2005). Such reduced fluids infiltrated unlithified BIF during the burial at Atlantis II Deep sediments (Red Sea), promoting the non-redox conversion of hematite to magnetite (Laurila et al. 2015). Thus, a variety of reactions under both hydrothermal and diagenetic conditions could have been responsible for the transformation of hematite to magnetite in the Glubochenskoe deposit.

Trace elements in magnetite can occur through isomorphic substitution or as mineral inclusions. In the Glubochenskoe deposit, the inner zone of magnetite grains (magnetite-1) is enriched in trace elements relative to the outer zones (magnetite-2) (ESM 6). The high concentrations of Si, Mg, Al, Na, and K contents in magnetite-1 samples most likely reflect the presence of inclusions of quartz, chlorite, and illite (Fig. 9). The variable higher Ti, Ca, Na, and P contents in magnetite-1 indicate the presence of rutile, leucoxene, carbonates, albite, and apatite inclusions. Some elements (Rb, Sr, U, Zr, and Y), probably reflect gangue mineral inclusions in magnetite, indicated by positive correlations between these elements and others such as Si and K (Fig. 9). The presence of inclusions of gangue minerals in the inner zones of magnetite grains suggests that they were enclosed during the decomposition of primary volcaniclastic minerals. Critical reactions may have included the decomposition (hydrolysis/dissolution) of volcanic glasses and primary igneous minerals (feldspars, pyroxene, olivine, amphibole, plagioclase, and titanomagnetite), and leaching of Ca^{2+}, Mg^{2+}, Fe^{2+} Al^{3+}, Ti^{4+}, Si^{4+}, and bicarbonate ions (Seyfried and Bishoff 1979; Petrova et al. 1980; Staudigel and Hart 1983; Flick et al. 1990). Additionally, iron may be fixed in volcaniclastic sediments by oxidation of Fe(II) dissolved in seawater to form an insoluble hydrous oxide precipitate (Ayres 1972; Flick et al. 1990).

The high Si contents (up to 0.09 wt%) may point to incorporation of some Si in the structure of magnetite (ESM 5) as a result of precipitation of Fe–Si aggregates in unlithified sediments. This may indicate that Si was primarily incorporated into hematite during lithification and further into magnetite under reducing conditions during late diagenesis, accompanied by reduction of Fe^{3+} into Fe^{2+}.

Magnetite of the Glubochenskoe deposit contains V and Ga, which could be absorbed by Fe oxyhydroxides from bottom waters during the decomposition of volcaniclastic material in the presence of organic matter and then incorporated into the structure of hematite and/or magnetite (Watson 1996).

Although mineral inclusions reflect the formation conditions of magnetite and give a direct insight into the evolution of the corresponding host rock, they skew the chemical analyses of magnetite (Nadoll et al. 2014). This is most likely the main reason that the compositional fields of magnetite-1 from the Glubochenskoe deposit on Ti vs. Ni/Cr and Al+Mn vs. Ti+V plots overlap with those of magnetite from different types of mineral deposits (Fig. 12a, b). Anomalously high Ti, V, Al, Mn, Cr, Ni, Sn, and Ga contents in magnetite are typical of high-temperature hydrothermal and igneous deposits (Dupuis and Beaudoin 2011; Nadoll et al. 2014; Dare et al. 2014; Knipping et al. 2015; Deditius et al. 2018). Low trace element (Mn, Ni, Cr, Sn) contents in magnetite-2 (ESM 6) are even lower than those of BIF magnetite, which is typically depleted in trace elements (Dupuis and Beaudoin 2011; Nadoll et al. 2014). The Ga contents in magnetite from the Glubochenskoe deposit are significantly higher relative to BIF magnetite (Fig. 12d). At the same time, due to relatively lower ranges in concentrations of many trace elements in magnetite-2, its compositional field is restricted in some discriminant diagrams (Fig. 12a, b). On plots of Ti+V vs. Ni/(Cr+Mn)

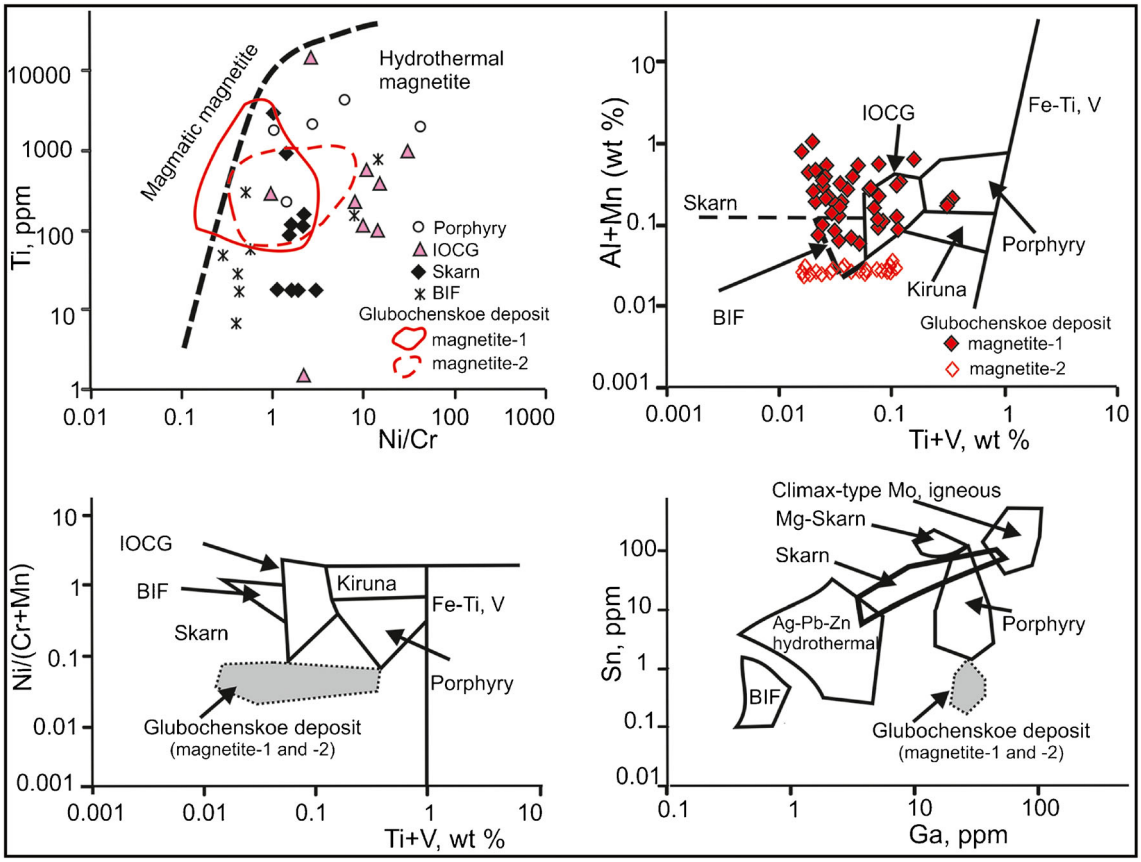

Fig. 12 Ti (ppm) vs. Ni/Cr (**a**), Ti+V vs. Al+Mn (**b**), Ti+V vs. Ni/(Cr+Mn) (**c**), and Ga vs. Sn (**d**) plots (Dupuis and Beaudoin 2011; Nadoll et al. 2014) for magnetite from the Glubochenskoe deposit. BIF: banded iron formation. Skarn: Fe–Cu skarn deposits. IOCG: iron oxide-copper-gold deposits. Porphyry: porphyry Cu deposits. Kiruna: Kiruna apatite-magnetite deposits. Fe–Ti, V: magmatic Fe–Ti-oxide deposits

and Ga vs Sn (Fig. 12c, d), the combined field for magnetite-1 and magnetite-2 is distinct from those of magnetite from skarn, IOCG, and metamorphosed BIF deposits.

Sulfide mineralization

The trace element composition of pyrite can contribute to an understanding of the genesis of iron deposits (Deditius et al. 2009; Qiang et al. 2009; Reich et al. 2016). The variable Co and Ni contents and Co/Ni ratios of pyrite from the Glubochenskoe deposit are related to the presence of two pyrite generations: an early porous core and a late homogeneous outer zone (Fig. 7k; ESM 7). Both morphology of pyrite and its trace element composition support its precipitation from diagenetic fluids in the siliciclastic sediments after sedimentation. The zoned pyrite could have formed during metamorphism with enlargement of pyrite grain size due to post-depositional fluid rock interaction (McClay and Ellis 1983; Craig et al. 1998).

Co/Ni ratios have been used to discriminate between submarine exhalative (Co/Ni 5–50), magmatic (Co/Ni 1) and sedimentary (Co/Ni < 1) pyrite (Bralia et al. 1979; Bajwah et al. 1987; Koglin et al. 2010; Large et al. 2011). However, it is apparent that the Co/Ni ratio alone is not a key for depositional conditions of pyrite, since Co/Ni ratios in pyrite from various iron deposit types overlap (Fig. 3 in Bajwah et al. 1987). For example, pyrite from the Xinqiao stratiform Cu–S–Fe–Au deposit has low contents of Co (0.76–63.32 ppm) and Ni (0.48–19.53 ppm) and Co/Ni ratios are 0.67–3.24, indicating a hydrothermal origin (Zhang et al. 2017). Pyrite from the Los Colorados IOA deposit in the Chilean Iron Belt has high Co, Ni, and As contents (~ 1 wt%) with Co/Ni ratios of > 2, suggesting a magmatic-hydrothermal origin (Reich et al. 2016). The Co/Ni ratio > 26 for pyrite from the Songhu iron deposit (China) indicate a volcanic exhalative sedimentary origin of this deposit (Qiang et al. 2009). At the Songhu deposit, the early sedimentary framboidal pyrite was recrystallized by hydrothermal fluids, accompanied by increasing Co contents and Co/Ni ratios.

In magnetite ores from the Glubochenskoe deposit, pyrite has different Co/Ni ratios: (i) < 1 in the core (pyrite-1) and (ii) 1.00–28.85 in the outer zone (pyrite-2) (ESM 7). Large et al. (2011) suggested that high Co/Ni ratio (> 1) of late pyrite in black shale-hosted gold deposits indicates interaction between sulfides and fluids during metamorphic modification of sediments with retention and even enrichment in Co and Ni. The

reducing conditions and organic matter favor the uptake by pyrite of more Ni than Co and the presence of Ni in sedimentary pyrites is unaffected by metamorphism and hydrothermal processes (Large et al. 2011). The additional factors controlling variable Co/Ni ratios (0.24–28.85) of pyrite from the Glubochenskoe deposit (Fig. 10a) are probably temperature and S fugacity, when increasing f_{S2} and/or decreasing temperature favor substitutions of first Co^{2+} and then Ni^{2+} for Fe^{2+} in pyrite (Maslennikov et al. 2009).

S, C, and O isotope constraints

The $\delta^{34}S$ values of pyrite (− 4.5 to + 3.6‰) from the Glubochenskoe deposit are similar to pyrite from the Kachar (− 3.3 to + 1.4), Sokolovskoe (− 2.7 to + 2.8), and Sarbai (+ 3.8 to + 0.9‰) skarn deposits of the Turgai belt (Hawkins et al. 2017) (Fig. 11a). Proponents of a skarn metasomatic model for the Turgai iron ores explain $\delta^{34}S$ values close to zero by magmatic sulfur source ($\delta^{34}S$ = 0 ± 2‰, Hawkins et al. 2017), as proposed for most skarn deposits ($\delta^{34}S$ = − 5‰ to + 8‰; e.g., Zhao et al. 2012; Bowman 1998). In case of the Glubochenskoe deposit, a wide range of $\delta^{34}S$ values (− 4.5 to + 3.6‰; ESM 8) in pyrite from magnetite ores most likely reflects the zoned structure of pyrite, in which the diagenetic core (pyrite-1) and the metamorphic rim (pyrite-2) are probably characterized by different $\delta^{34}S$ values. The two negative $\delta^{34}S$ values from layered samples (as low as − 4.5‰) can be interpreted to be derived from organic matter of clastic sedimentary rocks similarly to Japanese iron skarn deposits with relatively ^{34}S-depleted sulfur (− 5.4‰) (Shimazaki 1985).

The $\delta^{13}C$ values of carbonate minerals from the Glubochenskoe deposit differ from those of magmatic and skarn deposits and all marine limestones (Fig. 11b). The low $\delta^{13}C$ values of siderite from the Glubochenskoe deposit are most likely related to the oxidation of sedimentary organic material within the host rocks. In general, the presence of C-bearing siltstones suggests that the decomposition of organic matter of calcareous-volcaniclastic layers, the release of CO_2, and the changes in redox conditions (from oxidative to reducing) were important in the formation of siderite (Hangari et al. 1980). The extensive deposition of magnetite can be result of oxidation of organic matter coupled to the reduction of Fe (III) (Roberts 2015). The light $\delta^{13}C$ values in iron-rich carbonates record evidence for diagenetic reduction of ferric oxide precursors to magnetite and carbonate through microbial iron respiration (Walker 1984; Baur et al. 1985). The generally low $\delta^{13}C$ values of carbonates of microbially altered basaltic glass are attributed to metabolic by-products of bacteria, which oxidize the dissolved organic matter of pore waters (Banerjee et al. 2004). Some iron deposits that form in shallow environments can show relatively wide ranges of $\delta^{13}C$ values (Shimazaki et al. 1986). The interaction between organic C and P during alteration of calcareous-volcaniclastic material resulted in the formation of phosphates (apatite, monazite, and xenotime) in magnetite ores of the Glubochenskoe deposit. Such phosphates precipitate from pore waters with pH < 7, possibly through the aid of microbial activity (Gross and Berndt 2002).

The variable $\delta^{18}O$ values are significantly lower than those of marine carbonates (+ 23‰ SMOW) (Veizer and Hoefs 1976) and are also distinct from those of carbonates from other Turgai iron deposits (Fig. 11b) (Hawkins et al. 2017). The wide range in $\delta^{18}O$ values of carbonates from the Glubochenskoe deposit (from + 2.4 to + 17.4‰) was probably caused by isotopic exchange with local host rocks (between marine carbonates and clastic silicates) in the absence of pervasive fluids during regional metamorphic events (Valley 1986).

Evidence for a volcanic contribution to the formation of magnetite ores

It is considered that intermittent volcanic eruptions and the residual heat from emplaced subvolcanic intrusions can sustain low-temperature hydrothermal activity on the modern seafloor (Exon and Cronan 1983; Kelley et al. 2002; Pirajno 2009). In such scenarios, Fe oxyhydroxides precipitate at low temperatures from hydrothermal fluids exhaled on the seafloor. Metals are sourced from deep-seated hydrothermal convection and leaching at depth.

In our study, however, we suggest that the Fe-rich volcanic clasts can also be a major source of iron leached by seawater. We propose that the alternating deposition of Fe-poor (volcaniclastic) and Fe-rich (hematite) layers on the seafloor was due to pH variations and temperature fluctuations.

Sedimentological features within calcareous-volcaniclastic layers of the Glubochenskoe deposit can be used to infer seafloor conditions during mineral formation. The clastic material in volcaniclastic layers is a result of volcanic eruptions. In magnetite and calcareous-volcaniclastic layers, the original volcaniclastic material composed of volcanic glass, Fe–Mg silicates, Ti-minerals, feldspar group minerals, and lithic clasts display seafloor and diagenetic multistage alteration features (ESM 9). It is assumed that the volcaniclastic layers contained significant amounts of Fe prior to the formation of Fe-rich layers. At low seafloor temperatures, reactions occurred within seawater, and volcanic clasts mixed with carbonate and organic matter that would be favorable for the fixation of iron hydroxides (Maslennikov et al. 2012; Ayupova et al. 2017). Additionally, iron may be fixed in volcaniclastic sediments by oxidation of Fe(II) dissolved in seawater to form an insoluble hydrous oxide precipitate (Ayres 1972; Flick et al. 1990).

From this viewpoint, the ferric iron minerals (derived from volcaniclastic material) were oxidized and then rapidly

hydrolyzed to ferric hydroxide. In addition to the precipitation of colloidal and amorphous Fe oxyhydroxide phases, the alteration of volcanic glasses, Fe–Mg silicates, and titanomagnetite was followed by the formation of amorphous silica, smectite, and Ti phases, which have been transformed into chlorite, quartz, anatase (leucoxene), and illite during lithification (Ahn and Peacor 1985; Velde and Medhioub 1988; Drits and Kossovskaya 1989; Jahren and Aagaard 1989; Maslennikov et al. 2012). Such an environment would be favorable for the fixation of iron hydroxides in an open system, including the presence of oxygen and calcic material (Maslennikov et al. 2012; Ayupova et al. 2017).

Authigenic fibrous and laminar Fe chlorite may form locally as a result of the precursor smectite (Ahn and Peacor 1985; Beaufort et al. 2015). The calculated formation temperatures of Fe chlorite (184–217 °C; ESM 3) of magnetite layers from the Glubochenskoe deposit are consistent with the transformation of smectites during increasing temperatures from diagenesis. The late Fe–Mg chlorite and illite assemblage formed under slightly higher temperatures of 225–266 °C (ESM 3) and may be related to metamorphism. It is considered that the Fe–Mg chlorite and illite form as a result of the complete decomposition of pyroxene at increasing Mg activity and can coexist over a large range of K activity (Jahren and Aagaard 1989). In diagenetic systems, chlorite forms at temperatures of 100–120 °C for Mg-chlorite opposed to 40–120 °C for Fe chlorite (Beaufort et al. 2015). Unstable smectites and mixed-layered clays (smectite/chlorite, smectite/illite) formed during early burial are transformed to illite or chlorite during late diagenesis (Velde and Medhioub 1988; Jahren and Aagaard 1989). In typical argillaceous sediments, detrital smectite is replaced by chlorite and illite during burial metamorphism (Ahn and Peacor 1985).

The processes of dissolution and alteration of feldspars release K and Al from K-feldspar and those may then be incorporated in illite (Fig. 8e). Detrital feldspars can be unstable in diagenetic environments and alter by dissolution (Moncure et al. 1984) and/or replacement by clay minerals (Morad and Aldahan 1987), quartz, and albite (Walker 1984). This alteration may be due to the fluids, which easily penetrate the crystals along the crystallographic plains (e.g., twinning or cleavage) or cracks. The albitization of Ca-plagioclase from volcanosedimentary sequences is a very common diagenetic process that occurs at temperatures of 120–150 °C (Baccar et al. 1993).

Carbonate material in volcaniclastic layers of the Glubochenskoe deposit was likely sourced from erosion of nearby shallow limestone edifices. The formation of authigenic carbonates in layered ores is intimately linked to the dissolution of limestone clasts mixed with clay products during increasing temperatures of lithogenesis (Morse and Mackenzie 1990). Calcium, which was released during the albitization of feldspar (Ramseyer et al. 1992), became part of the pore fluids and was precipitated as authigenic calcite or Fe–Mg carbonate.

The formation of siderite, a major carbonate phase of the magnetite layers, can be interpreted as a product of the degradation of organic matter. This would have occurred through iron reduction of sulfate-poor ferruginous fluids in sediments (Maynard 1983). Siderite can precipitate from a mineralizing fluid during the conversion of the precursor iron oxides to magnetite (Gregory et al. 1989).

Conclusions

The stratiform magnetite bodies of the Glubochenskoe deposit accumulated in a submarine setting are conformable with calcareous-volcaniclastic layers and contain well-preserved fine-grained hematite layers up to 1–2 mm thick. The primary igneous components (volcanic glass, Ca–Mg silicates, titanomagnetite) of volcaniclastic layers underwent submarine weathering and leaching and could be a major source of iron in this deposit. The altered gangue clasts are consistent with seafloor replacement models (i.e., halmyrolysis). Based on the mineral assemblages and calculated formation temperature of chlorite, the iron ores underwent diagenesis and low-temperature metamorphism up to 266 °C (i.e., greenschist facies conditions).

The highly variable Si, Al, Mg, Na, K, Ca, Ti, Mn, Rb, Zr, Y, Sr, U, and P contents within magnetite-1 are related to the inclusions of gangue minerals (chlorite, illite, albite, carbonate, albite, leucoxene, rutile, apatite). Vanadium, Ga, Sc, Co, Ni, Ge, As, Cr, Mo, Sn, and W are most likely incorporated into the structure of magnetite-1 being absorbed by primary Fe oxyhydroxides from bottom waters during the decomposition of volcaniclastic material. The element contents (except V and Ga) in magnetite-2 are lower than in magnetite-1 as effect of depletion of late diagenetic fluids in elements. The presence of illite, Fe–Mg chlorite, rutile, and finely zoned magnetite-3 and porphyroblasts of magnetite indicate the late diagenetic and low-grade metamorphic transformations of early diagenetic components of iron ores. Using of discriminant diagrams based on the contents and ratios of main trace elements (Al, Ti, etc.) of magnetite from similar deposits would have no sense in case of numerous mineral inclusions in magnetite, thus requiring data on isomorphic trace elements (Ga, Sn, V, etc.).

The low $\delta^{13}C$ values (− 8.5 to − 19.5‰ PDB) of siderite from magnetite ores indicate that the decomposition of organic matter in calcareous-volcaniclastic layers, the release of CO_2, and the change oxidative to reducing conditions were important in the formation of siderite. The range of $\delta^{18}O$ values was probably caused by isotopic exchange with local host rocks in the absence of pervasive fluid during regional metamorphic events. The $\delta^{34}S$ variations (− 4.5 to + 3.6‰) of pyrite at the Glubochenskoe deposit can indicate either multistage pyrite formation and/or alteration processes during diagenesis and, possibly, metamorphism.

Acknowledgments The authors are grateful to Ivan Blinov (IMin) for SEM study of minerals and Irina Gottman (IGG UB RAS) for EPMA studies of magnetite. The authors thank Dr. Craig Johnson (USGS) and Dr. Martin Reich (University of Chile) for their valuable suggestions and Associate Editor Karen Kelley for recommendations and language adaptation, which improved this paper. Careful reading by Georges Beaudoin, Editor-in-Chief of Mineralium Deposita, is also greatly appreciated.

Funding information This work was supported by State Contract of the IMin (no. AAAA-A19-119061790049-3). SPH is currently funded by Geological Survey Ireland/DCCAE Postdoctoral Fellowship Program, No. 2016-PD-003.

References

Ahn JH, Peacor DR (1985) Transmission electron microscopic study of diagenetic chlorite in Gulf Coast argillaceous sediments. Clay Clay Miner 33:228–236

Alirezaei S, Cameron EM (2001) Variations of sulfur isotopes in metamorphic rocks from Bamble Sector, southern Norway: a laser probe study. Chem Geol 181:23–45. https://doi.org/10.1016/S0009-2541(01)00266-2

Ayres DE (1972) Genesis of iron-bearing minerals in banded iron formation mesobands in the Dales Gorge Member, Hamersley Group, Western Australia. Econ Geol 67:1214–1233

Ayupova NR, Maslennikov VV, Tessalina SG, Shilovsky OP, Sadykov SA, Hollis SP, Danyushevsky LV, Safina NP, Statsenko EO (2017) Tube fossils from gossanites of the Urals VHMS deposits, Russia: authigenic mineral assemblages and trace element distributions. Ore Geol Rev 85:107–130. https://doi.org/10.1016/j.oregeorev.2016.08.003

Baccar MB, Fritz B, Made B (1993) Diagenetic albitization of K-feldspar and plagioclase in sandstone reservoirs: thermodynamic and kinetic modeling. J Sediment Petrol 63(6):1100–1109

Bajwah ZU, Seccombe PK, Offier R (1987) Trace element distribution, Co:Ni ratios and genesis of the Big Cadia iron-copper deposit, New South Wales, Australia. Mineral Deposita 22:292–300

Banerjee NR, Furnes H, Muehlenbachs K, Staudigel H (2004) Microbial alteration of volcanic glass in modern and ancient oceanic crust as a proxy for studies of extraterrestrial material. Lunar and Planetary Science XXXV. 1248 pdf. https://doi.org/10.1016/j.epsl.2005.11.011

Baur ME, Hayes JM, Studley SA, Walter MR (1985) Millimeter scale variations of stable isotope abundance in carbonate from banded iron formations in the Hamersley group of Western Australia. Econ Geol 80:270–282

Beaufort D, Rigault C, Billon S, Bil V (2015) Chlorite and chloritization processes through mixed-layer mineral series in low temperature geological systems – a review. Clay Miner 50:497–523. https://doi.org/10.1180/claymin.2015.050.4.06

Bekmukhametov AE (1987) Magmatic iron formation. Nedra, Moscow (in Russian)

Belevtsev YN, Buharov VP, Naumenko VV, Goncharuk AF, Popov BA, Stepanov VA, Usenko AI (1982) About volcanogenic-sedimentary origin of magnetite ores of Urals. Geol Ore Dep 1:53–75 (in Russian)

Bontognali TRR, Fischer WW, Föllm KB (2013) Siliciclastic associated banded iron formation from the 3.2 Ga Moodies Group, Barberton Greenstone Belt, South Africa. Precambrian Res 226:116–124

Bowman JR (1998) Stable isotope systematic of skarns. In: Lentz, DR (Ed.) Mineralized intrusion-related Skarn systems. Short course series 26. Min Assoc Canada, Quebec, pp 99–146

Bralia A, Sabatini G, Troja F (1979) A revaluation of the Co/Ni ratio in pyrite as geochemical tool in ore genesis problems. Mineral Deposita 14:353–374

Brown DA, Gross GA, Sawicki JA (1995) A review of the microbial geochemistry of banded iron-formations. Can Mineral 33:1321–1333

Brown D, Puchkov V, Alvarez-Marron J, Bea F, Perez-Estaun A (2006) Tectonic processes in the Southern and Middle Urals: an overview. In: Gee DG, Stephenson RA (eds) European Lithosphere Dynamics 32, vol 32. Geological Society, London, Memoirs, pp 407–419. https://doi.org/10.1144/GSL.MEM.2006.032.01.24

Craig JR, Vokes FM, Solberg TN (1998) Pyrite: physical and chemical textures. Mineral Deposita 57:3–18. https://doi.org/10.1007/s001260050187

Cuadros J, Michalski JR, Dekov V, Bishop J, Fiore S, Dyar MD (2013) Crystal-chemistry of interstratified Mg/Fe-clay minerals from seafloor hydrothermal sites. Chem Geol 360–361:142–158. https://doi.org/10.1016/j.chemgeo.2013.10.016

Dare SAS, Barnes S-J, Beaudoin G, Méric J, Boutroy E, Potvin-Doucet C (2014) Trace elements in magnetite as petrogenetic indicators. Mineral Deposita 49:785–796. https://doi.org/10.1007/s00126-014-0529-0

Deditius AP, Utsunomiya S, Ewing RC, Chryssoulis SL, Venter D, Kesler SE (2009) Decoupled geochemical behavior of As and Cu in hydrothermal systems. Geology 37:707–710. https://doi.org/10.1130/G25781A.1

Deditius AP, Reich M, Simon A, Suvorova A, Knipping J, Roberts MP, Rubanov S, Dodd A, Saunders M (2018) Nanogeochemistry of hydrothermal magnetite. Contrib Mineral Petrol 173(6):46. https://doi.org/10.1007/s00410-018-1474-1

Drits VA, Kossovskaya AG (1989) Smectites-indicators of geological environments of continents and oceans. In: Halodov VN (ed) Genesis of sediments and fundamental problems of lithology. Nauka, Moscow, pp 7–37 (in Russian)

Dupuis C, Beaudoin G (2011) Discriminant diagrams for iron oxide trace element fingerprinting of mineral deposit types. Mineral Deposita 46:319–335. https://doi.org/10.1007/s00126-011-0334-y

Dymkin AM, Prugov VP (1980) Stratiform type of iron ores and their genetic signature. Nauka, Moscow (in Russian)

Exon NF, Cronan DS (1983) Hydrothermal iron deposits and associated sediments from submarine volcanoes off Vanuatu, southwest Pacific. Mar Geol 52(3-4):M43–M52. https://doi.org/10.1016/0025-3227(83)90052-X

Fischer WR, Schwertmann U (1975) The formation of hematite from amorphous iron(III)hydroxide. Clays Clay Min 23:33–37. https://doi.org/10.1346/ccmn.1975.0230105

Flick H, Nesbor HD, Behnisch R (1990) Iron ore of the Lahn-Dill type formed by diagenetic seeping of pyroclastic sequences – a case study on the Schalstein section at Gänsberg (Weilburg). Geol Rundsch 79(2):401–415

Gregory RT, Criss RE, Taylor HP Jr (1989) Oxygen isotope exchange kinetics of mineral pairs in closed and open systems: applications to problems of hydrothermal alteration of igneous rocks and Precambrian iron formations. Chem Geol 75:1–42. https://doi.org/10.1016/0009-2541(89)90019-3

Gross KA, Berndt CC (2002) Biomedical application of apatites. In Kohn MJ, Rakovan J, Hughe JM (eds) Phosphates. Geochemical, geobiological, and materials importance 48: 631–672

Hangari KM, Ahmad SN, Perry EC (1980) Carbon and oxygen isotope ratios in diagenetic siderite and magnetite from Upper Devonian ironstone, Wadi Shatti District, Libya. Econ Geol 75(4):538–545. https://doi.org/10.2113/gsecongeo.75.4.538

Hawkins T, Smith MP, Herrington RJ, Maslennikov VV, Boyce AJ, Jeffries T, Creaser RA (2017) The geology and genesis of the iron skarns of the Turgai belt, northwestern Kazakhstan. Ore Geol Rev 85:216–246. https://doi.org/10.1016/j.oregeorev.2015.10.016

Herrington R, Smith M, Maslennikov V, Belogub E, Armstrong R (2002) A short review of Palaeozoic hydrothermal magnetite iron-oxide deposits of the south and central Urals and their geological setting. In: Porter TM (Ed.) Hydrothermal iron oxide copper-gold and related deposits: a global perspective 2. PGC Publishing, pp. 343–353, http://local.www.geokniga.org/books/4957

Ivlev AI (2004) The Kachar iron deposit – a new look at the geological structure. In: Ivlev AI (Ed): Toporkov readings. Rudniy, pp. 62–82 (in Russian)

Jahren JS, Aagaard P (1989) Compositional variations in diagenetic chlorite and illite, and relationships with formation-water chemistry. Clay Miner 2:157–170. https://doi.org/10.1180/claymin.1989.024.2.04

Kaufman AJ, Hayes JM, Klein C (1990) Primary and diagenetic controls of isotopic compositions of iron-formation carbonates. Geochim Cosmochim Acta 54:3461–3473. https://doi.org/10.1016/0016-7037(90)90298-Y

Kranidiotis P, MacLean WH (1987) Systematics of chlorite alteration at the Phelps Dodge massive sulfide deposit, Matagami, Quebec. Econ GeoL 82:1898–1911. https://doi.org/10.2113/gsecongeo.82.7.1898

Kelley DS, Baross JA, Delaney JR (2002) Volcanoes, fluids, and life at mid-ocean ridge spreading centers. Annu Rev Earth Planet Sci 30: 385–491

Kiyokawa S, Ueshiba T (2015) Rapid sedimentation of iron oxyhydroxides in an active hydrothermal shallow semi-enclosed bay at Satsuma Iwo-Jima Island, Kagoshima, Japan. Sediment Geol 319:98–113. https://doi.org/10.1016/j.sedgeo.2015.01.010

Knipping JL, Bilenker LD, Simon AC, Reich M, Barra F, Deditius AP, Wälle M, Heinrich CA, Holtz F, Munizaga R (2015) Trace elements in magnetite from massive iron oxide-apatite deposits indicate a combined formation by igneous and magmatic-hydrothermal processes. Geochim Cosmochim Acta 171:15–38. https://doi.org/10.1016/j.gca.2015.08.010

Koglin N, Frimmel HF, Lawrie Minter WE, Bratz H (2010) Trace-element characteristics of different pyrite types in Mesoarchean to Paleoproterozoic placer deposits. Mineral Deposita 45:259–280. https://doi.org/10.1007/s00126-009-0272-0

Kossovskaya AG, Petrova VV, Shutov VD (1982) The mineral associations of palagonitization of oceanic basalts and problems of extraction of ore components. Lithol Miner Resour 3:10–31

Large RR, Bull SW, Maslennikov VV (2011) A carbonaceous sedimentary source-rock model for Carlin-type and orogenic gold deposits. Econ Geol 106:331–358

Laurila T, Hannington M, Leybourne M, Peterson S, Devey CW, Garbe-Schoenberg D (2015) New insights into the mineralogy of the Atlantis II Deep metalliferous sediments, Red Sea. Geochem Geophys Geosyst 16:4449–4478. https://doi.org/10.1002/2015GC006010

Lu JF, Tsai CJ (2015) Reduction kinetics of hematite to magnetite under hydrothermal treatments. RSC Adv 22:17236–17244. https://doi.org/10.1039/c4ra12389a

Maslennikov VV, Maslennikova SP, Large RR, Danyushevsky LV (2009) Study of trace element zonation in vent chimneys from the Silurian Yaman-Kasy VHMS (the Southern Urals, Russia) using laser ablation inductively coupled plasma mass spectrometry (LA-ICP MS). Econ Geol 104:1111–1141

Maslennikov VV, Ayupova NR, Herrington RJ, Danyushevskiy LV, Large RR (2012) Ferruginous and manganiferous haloes around massive sulphide deposits of the Urals. Ore Geol Rev 47:5–41. https://doi.org/10.1016/j.oregeorev.2012.03.008

Maynard JB (1983) Geochemistry of sedimentary ore deposits. Springer-Verlag, New York

McClay KR, Ellis PG (1983) Deformation and recrystallisation of pyrite. Mineral Mag 47:527–538. https://doi.org/10.1180/minmag.1983.047.345.14

Moncure GK, Lahann RW, Siebert RV (1984) Origin of secondary porosity and cement distribution in a sandstone/shale sequence from the Frio Formation (Oligocene) / In: Clastic diagenesis (ed. D.A. Mc. Donald and R.C. Surdam). Mem Am Assoc Petrol Geol 37: 151–161

Morad S, Aldahan AA (1987) Diagenetic chloritization of feldspars in sandstones. Sediment Geol 51:155–164. https://doi.org/10.1016/0037-0738(87)90046-7

Morse JW, Mackenzie FT (1990) Geochemistry of sedimentary carbonates. Developments in sedimentology. Elsevier, Amsterdam

Mucke A, Cabral RA (2005) Redox and nonredox reactions of magnetite and hematite in rocks. Chem Erde 65:271–278. https://doi.org/10.1016/j.chemer.2005.01.002

Nadoll P, Angerer T, Mauk JL, French D, Walshe J (2014) The chemistry of hydrothermal magnetite: a review. Ore Geol Rev 16:1–32. https://doi.org/10.1016/j.oregeorev.2013.12.013

Ohmoto H, Rye RO (1979) Isotopes of sulfur and carbon. In: Barnes HJ (ed) Geochemistry of Hydrothermal Ore Deposits, 2nd edn. Wiley, New York, pp 509–567

Orlov VP (ed) (2007) Iron ore base of Russia. Geoinformmark, Moscow (in Russian)

Ovchinnikov LN, Dymkin AM (Ed) (1987) Iron ore formation of Transuralian zone (northern part of the Turgai trough). USC of Academy of Sciences USSR (in Russian)

Petrova VV, Voronin BI, Serebrennikova ND (1980) Features of the underwater change of the mafic glass in the core of 160 voyage of Glomar Challenger. Lithol Miner Resour 2:133–142 (in Russian)

Pirajno F (2009) Submarine hydrothermal mineral systems. In: Pirajno F (ed.): Hydrothermal processes and mineral systems, Springer, 1250 p.

Poltavets YA (2009) The Tyumen-Kustanay trough: features of magmatism and metallogeny. Lithosfera 3:17–32 (in Russian)

Porotov GS (1981) Connection of magnetite deposits of the Turgai trough with paleovolcanic structures. In: Geology and genesis of iron ore deposits. USSR Academy of Sciences, Sverdlovsk, pp. 25–34 (in Russian)

Posth NR, Konhauser KO, Kappler A (2013) Microbiological processes in banded iron formation deposition. Sedimentology 60:1733–1754. https://doi.org/10.1111/sed.12051

Puchkov VN (2013) Structural stages and evolution of the Urals. Mineral Petrol 107(1):3–37. https://doi.org/10.1007/s00710-012-0263-1

Qiang S, Zhang B, Yong L, Chang PZ, Xue YY, Qiao SZ, Wu BY, He CN (2009) Characteristics and trace element geochemistry of pyrite from the Songhu iron deposit, Nilek County, Xinjiang, China. Acta Petrol Sin 25(6):1456–1464

Ramdohr P (1969) Ore minerals and their intergrowhs. (Monographs in Earth Science). Oxford

Ramseyer K, Boles JR, Lichtner PC (1992) Mechanism of plagioclase albitization. J Sediment Petrol 62:349–356

Reed MH (1983) Seawater-basalt reaction and the origin of greenstones and related ore deposits. Econ Geol 78(3):466–485

Reich M, Simon AC, Deditius A, Barra F, Chryssoulis S, Lagas G, Tardani D, Knipping J, Bilenker L, Sánchez-Alfaro P, Roberts MP, Munizaga R (2016) Trace element signature of pyrite from the Los Colorados iron oxide-apatite (IOA) deposit, Chile: a missing link between Andean IOA and IOCG systems? Econ Geol 111:743–761. https://doi.org/10.2113/econgeo.111.3.743

Roberts AP (2015) Magnetic mineral diagenesis. Earth Sci Rev 151:1–47. https://doi.org/10.1016/j.earscirev.2015.09.010

Rudnitsky VF, Aleshin KB, Kuznetsov AZ, Ivanchenko VS (2013) Structure of magnetite lodes at the Estyunino iron deposit in the central Urals. Geol Ore Dep 55(6):467–481

Seyfried WE, Bishoff JL (1979) Low temperature basalt alteration by seawater: an experimental study at 70 and 150 °C. Geochim Cosmochim Acta 43:1937–1947

Shimazaki H (1985) Regional variation of isotopic composition of hydrothermal ore sulfur in Japan. J Fac Sci Univ Tokyo, Sect, II 21:81–100

Shimazaki H, Shimizu M, Takanori N (1986) Carbon and oxygen calcites from Japanese isotopes of skarn deposits. Geochem J 20:297–310

Staudigel H, Hart S (1983) Alteration of basaltic glass: mechanisms and significance for the oceanic crust-seawater budget. Geochim Cosmochim Acta 47:337–350. https://doi.org/10.1016/0016-7037(83)90257-0

Sturesson U (2003) Lower Palaeozoic iron oolites and volcanism from a Baltoscandian perspective. Sediment Geol 159(3):241–256. https://doi.org/10.1016/S0037-0738(02)00330-5

Taitel-Goldman N, Singer A (2002) Metastable Si-Fe phases in hydrothermal sediments of Atlantis II Deep, Red Sea. Clay Miner 37:235–248. https://doi.org/10.1180/0009855023720030

Valley JW (1986) Stable isotope geochemistry of metamorphic rocks. Rev Mineral Geochem 16(1):445–489

Veizer J, Hoefs J (1976) The nature of O^{18}/O^{16} and C^{13}/C^{12} secular trends in sedimentary carbonate rocks. Geochim Cosmochim Acta 40:1387–1395

Velde B, Medhioub M (1988) Approach to chemical equilibrium in diagenetic chlorites. Contrib. Mineral Petrol 98:122–127

Walker JCG (1984) Suboxic diagenesis in banded iron formations. Nature 309:340–342

Watson EB (1996) Surface enrichment and trace-element uptake during crystal growth. Geochim Cosmochim Acta 60:5013–5020. https://doi.org/10.1016/S0016-7037(96)00299-2

Zhang Y, Shao Y, Chen H, Liu Z, Li D (2017) A hydrothermal origin for the large Xinqiao Cu-S-Fe deposit, Eastern China: evidence from sulfide geochemistry and sulfur isotopes. Ore Geol Rev 88:534–549. https://doi.org/10.1016/j.oregeorev.2016.08.002

Zhao HJ, Xie GQ, Wei KT, Ke YF (2012) Mineral compositions and fluid evolution of the Tonglushan skarn Cu–Fe deposit, SE Hubei, east-central China. Int Geol Rev 54:737–764. https://doi.org/10.1080/00206814.2011.569418